Rainshadow effect on hydrogen isotopes in leaf wax n-Alkanes across the Cascade Mountains of Washington, USA

Hope Sisley, Matthew Wolhowe, Jon Rowe, Alexis Licht, Julian Sachs

Rainshadow Effect on Hydrogen Isotopes in Leaf Wax *n*-Alkanes across the Cascade Mountains of Washington, USA

Hope Sisley[1,*]

Matthew Wolhowe[2]

Jon Rowe[1]

Alexis Licht[1,3]

Julian Sachs[2]

[1] Department of Earth and Space Sciences, University of Washington, Seattle, WA 98195 USA

[2] School of Oceanography, University of Washington, Seattle, WA 98195 USA

[3] Aix Marseille University, CNRS, IRD, INRAE, Collège de France, CEREGE, Aix-en-Provence, France

*Corresponding author email: vortagal@uw.edu

Abstract

Hydrogen isotope ratios are sensitive tracers of the water cycle with the potential to constrain the timing of mountain building episodes in the geologic past. This study presents hydrogen isotope ratios ($^2H/^1H$ or δ^2H) of *n*-alkanes derived from the leaf wax of terrestrial plants, collected from trees and soils along an east-west transect across the Cascade mountain range of Washington State, USA. Along this transect, the δ^2H values of *n*-alkanes (δ^2H_{alkane}) in surface soils and gymnosperm leaves are well-correlated with the mean annual δ^2H of precipitation (δ^2H_{precip}) derived from instrument-model reanalysis products (R^2=0.346 to 0.558, $p<0.001$ for soil alkanes, R^2=0.667 to 0.844, $p<0.001$ for gymnosperm alkanes) and with measured δ^2H values of nearby surface waters (R^2=0.451, $p<0.001$). All data from this study show increasing deuterium (^2H) depletion with distance from the coast in response to Rayleigh distillation induced by the Cascade Mountains. Assessed within the context of a global dataset of 235 published soil δ^2H_{alkane} values vs. δ^2H_{precip}, the Cascades results are statistically indistinguishable. However, the gymnosperm leaf δ^2H_{alkane} vs. δ^2H_{precip} data from the Cascades differ from a global set of 87 such sites, with a steeper relationship. This is attributed to regional differences between the Cascades and other locations that include higher latitude, higher altitude, and the presence of a strong, narrow climatic gradient. The strong imprint of the Cascade rainshadow on δ^2H_{alkane} validates its use as a proxy for the timing of uplift of this mountain range when measured in suitable sedimentary rocks.

Keywords

Orogenic rain shadow, Cascade Mountains, gymnosperm *n*-alkanes, soil *n*-alkanes, δ^2H, d^2H, δD, dD, hydrogen isotopes, isotopic lapse rate.

1. **Introduction**

Long-chain hydrocarbons are a primary constituent of the waxy coating of plant leaves (Howard 2014), and their hydrogen isotopic composition ($^2H/^1H$ or δ^2H) reflects that of the local meteoric water (Sachse et al. 2012). Because δ^2H in atmospheric waters changes with altitude (Vogel et al. 1975), precipitation amount and type (Mook et al. 1974), distance from the nearest coast (Taylor 1972), latitude (Yurtsever 1975), extent of rainout (Roe 2005), and temperature (Dansgaard 1964, Mook 2001), the δ^2H value of a plant's *n*-alkanes (δ^2H_{alkane}) has the potential to provide information about all of these factors. *n*-Alkanes persist in soils following leaf abscission (Meyers et al. 1995, Huang et al. 1997, Nguyen-Tu et al. 2004) and become lithified (e.g. Volk et al. 2005, Marshall et al. 2007, Jarrett et al. 2019), allowing for the use of sedimentary δ^2H_{alkane} values as environmental and climatic proxies in paleoclimate reconstructions globally and across timescales from decades to millions of years (Polissar et al. 2009, Aichner et al. 2010, Hren et al. 2010, Collins et al. 2013, Jia et al. 2015, Niedermeyer et al. 2016, Lin et al. 2020).

Paleoclimate proxies like δ^2H_{alkane} require empirical validation owing to the large number of factors that influence (1) the generation of the isotopic signal in plants and (2) the preservation of that signal in sedimentary rocks. While the δ^2H value of a plant's water source is the primary control on its δ^2H_{alkane} value (Sachse et al. 2012), many other biological and environmental factors can influence a plant's δ^2H_{alkane}: plant species (Pedentchouk et al. 2008, Doman 2015, Feakins et al. 2016a), the time of year during which the alkane was produced (Kahmen et al. 2011, Tipple et al. 2013, Newberry et al. 2015, Sachse et al. 2015), plant functional type (gymnosperm vs. angiosperm, herbaceous vs. woody, deciduous vs. evergreen, etc.) (Yang et al. 2011a, Lane 2017), plant metabolic pathway (C3 vs. C4 vs. CAM) (Bi et al. 2005), aridity (Feakins and Sessions 2010, Douglas et al. 2012), mean annual temperature (MAT) (Tipple and Pagani 2013), mean annual precipitation (MAP) (Aichner et al. 2010, Nieto-Moreno et al. 2016, Feakins et al. 2018), relative humidity (Smith and Freeman 2006, Goldsmith et al. 2019), elevation (Jia et al. 2008, Bai et al. 2011, Zhang and Liu 2011, Ernst et al. 2013, Feakins et al. 2018) and local surface water δ^2H (Schwab et al. 2015). The process of senescence, diagenesis, and lithification - the transfer of the alkane from a living leaf into the rock record - can also affect δ^2H_{alkane} (Buggle 2011, Zech et al. 2011) or even destroy the alkanes outright (Allan and Douglas 1977, Kikuchi et al. 2010). Researchers have explored many of these uncertainties, examining the differences in δ^2H across species (e.g., Pedentchouk et al. 2008) and the changes

in δ^2H from living plant to leaf litter/duff (e.g., Zech et al. 2011). Studies have also been performed on modern plants across climatic gradients in order to evaluate the influence of different environmental effects on plant δ^2H_{alkane} (Tipple and Pagani 2013), but most of the studies examining a climatic gradient have dealt with arid or monsoonal climates (e.g., Douglas et al. 2012, Zhang et al. 2017), not temperate climates. Studies of rainshadow gradients, in particular, have concentrated on extreme environments such as the Andes (e.g., Nieto-Moreno et al. 2016), and none has been conducted on a strong temperate rainshadow like that found in the Pacific Northwest of North America.

The Cascade Mountains, which run north-south through Oregon and Washington into British Columbia, produce a large rainshadow effect (Fig. 1a): to the west of the Cascades, the Pacific Northwest consists primarily of temperate rainforest – dominated by mosses and ferns; evergreen shrubs such as salal, huckleberry, and Oregon grape; invasives such as Himalayan blackberry; and large coniferous trees, primarily Douglas fir, Western red cedar, and Western hemlock - while to the east are xeric open forest and dry scrubland, dominated by Ponderosa pine; sagebrush, antelope brush, and related shrubs; groundcovers such as kinnikinnick and falsebox; herbaceous flowering annuals such as balsamroot and lupine; C3 grasses such as bluebunch wheatgrass; and invasives such as hawksbeard and knapweed (Lyons and Merilees 1995). Bellingham, on the wet western side of the Cascades, receives an annual average of ~910 mm of precipitation, while Omak, on the dry eastern side, receives just 380 mm (NOAA normals 1981-2010), yet both these cities have a mean annual temperature of ~10 °C. The rainshadow is also relatively narrow at ~150 km across from east to west. The orographic precipitation that produces the east-west rainfall gradient is associated with Rayleigh distillation of water isotopes that causes a large isotopic gradient in precipitation across the range. On the windward (western) side of the Cascades, the mean annual δ^2H of precipitation (δ^2H_{precip}) averages between -60 and -80‰, while in eastern Washington, δ^2H_{precip} averages between -100 and -120‰ (IAEA/WMO 2017) (Fig. 1c). The δ^2H_{precip} gradient across the Cascade Mountains arises from the process of Rayleigh distillation in which ^2H_2O condenses from water vapor more readily than ^1H_2O. This gradient represents a complex environmental signal comprising multiple interdependent factors: distance from the coast (the continent effect) and elevation (the altitude effect), which are themselves expressions of ambient temperature and amount of rainout. As an air mass moves inland from the coast, it progressively loses deuterium to rainout, even if the continent is entirely

flat. Likewise, increasing altitude leads to a decrease in temperature, which leads to enhanced rainout of deuterium. The Cascade rainshadow is produced by the interplay of these two effects: the moisture-rich air is driven inland by the prevailing winds (which run west to east) and begins to lose deuterium immediately; but at the air mass encounters the Cascades, it is driven steeply upward, leading to a sharp drop in pressure and temperature. This drastically increases condensation and therefore rainout, further depleting the deuterium from the air mass. By the time the air mass crests the mountains and begins to sink into warmer, higher-pressure regimes on the east side, much deuterium has already been lost from the vapor. The Cascades do sit in the lee of the Olympic Mountains, which produce their own rainshadow, and the Okanogan Mountains to the east of the Cascades produce a muted rainshadow as well. Microclimates – such as narrow valleys between peaks – can also lead to noise in the isotopic signal, often at a sub-grid-level scale.

In an effort to determine the fidelity with which δ^2H_{alkane} values reflect δ^2H_{precip} across the Cascades mountain range, this study examines δ^2H_{alkane} in soils and living plants from 43 sites sampled from 2017-2019, as well as in two Tertiary rock samples from west of the modern Cascades, and how these values compare to δ^2H_{precip} values derived from the Oxygen Isotopes in Precipitation Calculator (OIPC) reanalysis (Bowen and Revenaugh 2003, Bowen 2017). In so doing, this study seeks to answer the following questions: (1) Is the δ^2H_{alkane} value of soils and plants from a temperate, cross-mountain environment predictive of local δ^2H_{precip}? (2) How does the relationship between δ^2H_{alkane} and δ^2H_{precip} across the Cascade Mountains compare to that relationship in a global compilation of δ^2H_{alkane} and δ^2H_{precip} values? and (3) Is the Cascades rainshadow effect visible in the δ^2H_{alkane} data? By answering these questions, we seek to establish whether changes in sedimentary δ^2H_{alkane} can be used to infer the timing of establishment of the Cascades rainshadow, and, by extension, the debated timing of the uplift of the Cascade mountain range.

2. **Methods**

From May to August 2019, plant and soil samples were collected from 45 sites across an 18-quadrant transect spanning northern Washington State (Fig. 1b); surface-water samples were collected at twelve of these sites. Plant samples included conifers from two major gymnosperm families: Cupressaceae (Western red cedar) and Pinaceae (larch, Ponderosa and lodgepole pine,

Douglas fir, Western hemlock, and several species of true fir); all of these are evergreens except the larch. From August to September 2018, 20 soil samples were collected across the same transect, and three other soil samples were collected in 2017 from further south (Fig. 1b). Sites were selected to be relatively flat in order to limit the potential impact of sediment transport; to not be immediately adjacent to a road, if possible, to minimize contamination from car exhaust and other human pollutants; to not be in a spot irrigated by humans, to avoid the isotopic influence of a water source other than atmospheric precipitation and natural surface waters fed by that precipitation; and to have not been recently burned, as wildfire can alter or destroy the soil's alkanes (Gonzalez-Perez et al. 2004). (Further details and an extensive overview of sampling protocols and procedure may be found in the Supplementary Material.) Two rock samples were also collected in 2017 to confirm (1) that enough viable *n*-alkanes could be recovered from local near-shore marine sedimentary rocks to allow reliable isotopic analysis and (2) whether the isotopic signature of these fossil *n*-alkanes is broadly compatible with modelled δ^2H_{precip}. Samples were collected from two marine sandstone outcrops at sea level on Bainbridge Island in western Washington, from the Miocene Blakeley Formation and the Oligocene Blakely Harbor Formation.

Alkane extraction, purification and δ^2H analysis was conducted according to procedures described in Nelson and Sachs (2013). Alkanes were extracted from freeze-dried sediment by pressurized fluid extraction with a Dionex ASE-200 and from leaf samples via sonication in dichloromethane, prior to purification on silica gel columns with elution in hexane. Individual *n*-alkane concentrations in each sample were quantified by gas chromatography with flame ionization detection (GC-FID) (Agilent 6890 GC). δ^2H_{alkane} values were measured with a Thermo Trace GC Ultra (Thermo Scientific, Waltham, MA, USA) connected to a Thermo Delta V isotope ratio mass spectrometer (IRMS) via a pyrolysis interface (Thermo-Fisher, Bremen, Germany). Isotope measurements are given as δ^2H values relative to Vienna Standard Mean Ocean Water (VSMOW). Water samples were analysed for δ^2H using a Picarro L2130-i Isotopic Liquid Water Analyzer with A0211 High-Precision Vaporizer (Picarro Inc., Santa Clara, CA). Data were compared to raster environmental data from the USGS (http://gis.ess.washington.edu/data/raster/thirtymeter/index.html), the PRISM climate database (http://prism.oregonstate.edu/normals/), and the OIPC database v3.1 (http://wateriso.utah.edu/waterisotopes/pages/data_access/ArcGrids.html). The OIPC data

product, like any large-scale gridded data assimilation, is prone to large uncertainties, with substantial sub-grid-scale real-world variations in elevation and measurements which the model does not account for; likewise, the original data upon which the model is based are extremely sparse over the Pacific Northwest. The standard deviations for δ^2H_{precip} provided by the OIPC incorporate these sources of uncertainty.

A compilation of all known gymnosperm δ^2H_{alkane} data in publication (as of August 31, 2020) yielded 23 studies, comprising 87 unique sites and 235 individual data points over three continents, and representing 14 genera from 5 families. In order to maximize the number of data points, the unweighted average δ^2H_{alkane} of all chain lengths (nC21 to nC35) for which the authors provided data was used to represent gymnosperm δ^2H_{alkane} in regression analyses. Estimated mean annual δ^2H_{precip} values were calculated for each site using the online OIPC calculator (http://wateriso.utah.edu/waterisotopes/pages/data_access/oipc.html) and missing location data were filled in using Google Earth Pro (version 7.3.3.7699). (See Supplementary Material for additional methods details.)

3. **Results**

δ^2H data was obtained for 36 soil samples (Supplementary Table 1), 14 gymnosperm samples (Supplementary Table 2), two rock samples (Supplementary Table 3), and 12 surface water samples (Supplementary Table 4) from a total of 44 spatiotemporal sites (Supplementary Table 5). δ^2H values for each odd chain-length *n*-alkane (nC23 to nC35) are reported as the average of replicate isotopic analyses (n=1 to 5, average n=3), and site averages (Supplementary Table 6) were calculated from these values. Ordinary least-squares regression yielded a strong correlation ($R^2>0.75$) between elevation and MAT and a weak correlation ($0.5>R^2>0.25$) between distance along transect from west to east (DAT) and MAP, as well as moderate correlations ($0.75>R^2>0.5$) of δ^2H_{precip} with elevation, DAT, and MAT. (R^2 values from ordinary least-squares regressions can be found in Supplementary Table 7 and p-values in Supplementary Table 8.) While the number of surface water samples (n=7) was too low to indicate significance, surface water δ^2H correlated moderately to strongly with average soil δ^2H_{alkane}. The δ^2H_{alkane} of all chain lengths (soil and gymnosperm) and all averages correlated with δ^2H_{precip} except gymnosperm nC23, which was uncorrelated (Supplementary Fig. 1); strong to moderate correlations with δ^2H_{precip} were seen with gymnosperm δ^2H_{alkane}, while soil δ^2H_{alkane} exhibited

moderate to weak correlations with δ^2H_{precip} (Fig. 2). DAT correlated with δ^2H_{alkane} of all chain lengths except nC23 (no correlation) and with the average δ^2H_{alkane} of both soils and gymnosperms (Supplementary Fig. 2): strong to moderate correlations with gymnosperms and moderate to weak correlations with soils. MAT correlated moderately with soil nC23 alkane δ^2H and weakly with soil nC25 alkane δ^2H, but not with any other soil δ^2H_{alkane} values. Gymnosperms, on the other hand, correlated moderately to weakly with MAT in nC27, nC29 and nC31 alkane δ^2Hs and in average δ^2H_{alkane} (Supplementary Fig. 3).

The Cascades data and OIPC mean annual δ^2H of precipitation were also compared via type-2 weighted linear regression (Supplementary Fig. 4), as both data sets carry large uncertainties. The analysis produced p-values >0.6 for δ^2H_{alkane} for all chain lengths in both soils and gymnosperms, for average δ^2H_{alkane} of both soils and gymnosperms, and for surface water δ^2H. Ordinary least squares regression, however, was necessary for comparison of the Cascades data to the literature, as <10% of published gymnosperm δ^2H_{alkane} data reported estimates of uncertainty.

Least-squares regression of published gymnosperm δ^2H_{alkane} data shows that, globally, gymnosperm δ^2H_{alkane} values correlate positively but weakly with the estimated annual average δ^2H_{precip} (R^2=0.263, p<0.001; slope=0.37) (Fig. 2). However, this trend is strongly influenced by a single outlier study, Zhang et al. (2017), which exhibits no correlation between δ^2H_{alkane} and δ^2H_{precip} (R^2=0.163, p=0.832). When Zhang et al. (2017) is removed from the analysis, global gymnosperm δ^2H_{alkane} correlates moderately with δ^2H_{precip} (R^2=0.449, p<0.001) and has a steeper positive relationship (slope=0.62) (Fig. 3a). Addition of the Cascades data (this study) to the literature data strengthens this relationship, increasing the positive correlation and the steepness of the slope of the relationship (without Zhang et al. 2017: R^2=0.669, p<0.001, slope=0.798; with Zhang et al. 2017: R^2=0.463, p<0.001, slope=0.596). Regionally, the relationship between δ^2H_{alkane} and δ^2H_{precip} varies strongly (Fig. 3a), though only Asia, eastern North America, and western North America have enough sites with gymnosperm δ^2H_{alkane} data to allow for meaningful regression. Phylogeny may also have an effect on how well the δ^2H_{alkane} value of a given gymnosperm reflects the estimated annual average δ^2H_{precip}; when the two major gymnosperm families are compared separately to annual δ^2H_{precip}, Pinaceae has essentially no correlation with δ^2H_{precip} (R^2=0.077, p=0.5), whereas Cupressaceae has a weak to moderate positive correlation (R^2=0.301, p<0.001; slope=0.42; intercept=-121) (Fig. 3b). If the Zhang et

al. (2017) data are removed from the analysis, however, Pinaceae δ^2H_{alkane} exhibit a nearly-identical relationship to δ^2H_{precip} (R^2=0.234, p<0.001; slope=0.42; intercept=-145) as Cupressaceae. When sites from the Cascades study that include δ^2H_{alkane} data from only a single gymnosperm family are combined with the literature data, and Zhang et al. (2017) is excluded, the correlation between Pinaceae δ^2H_{alkane} and δ^2H_{precip} improves (R^2=0.358, p<0.001; slope=0.65) (Fig. 3b).

Gymnosperm δ^2H_{alkane} values from the literature are significantly correlated with MAT (R^2=0.36, p<0.001; n=70) (Supplementary Fig. 3). The addition of the Cascades data to the literature data improves the MAT correlation (R^2=0.507, p<0.001). Latitude has a weak negative relationship with gymnosperm δ^2H_{alkane} whether Zhang et al. (2017) is included (R^2=0.282, p<0.001) or not (R^2=0.364, p<0.001) (Supplementary Fig. 5). The Cascades data slightly increase the correlation, whether Zhang et al. (2017) is included (R^2=0.42, p<0.001) or not (R^2=0.477, p<0.001).

Apparent fractionation factors (alpha) were calculated for the Cascades, comparing each chain length of soil δ^2H_{alkane} (Cascades only; Supplementary Table 10) and gymnosperm δ^2H_{alkane} (Supplementary Table 11), as well as gymnosperm δ^2H_{alkane} from the literature (Supplementary Table 12), to both δ^2H_{precip} and surface water δ^2H. In the Cascades, alpha for gymnosperm C29 and C31 δ^2H_{alkane} correlated weakly with elevation (C29: R^2=0.453, p=0.008; C31: R^2=0.427, p=0.015). For literature gymnosperm δ^2H_{alkane}, alpha correlated weakly to moderately with elevation for all chain lengths 25-31, but this correlation disappears when Zhang et al. (2017) is excluded from the analysis (Fig. 4). Likewise, alpha of gymnosperm family Pinaceae (including both literature and Cascades data) correlates with elevation for all chain lengths 25-31 (p<=0.001), but only for C29 and C31 when Zhang et al. (2017) is excluded; alpha for family Cupressaceae (including the Cascades) correlates weakly with elevation only for C33 and C35 δ^2H_{alkane} (Supplementary Fig. 6).

4. **Discussion**

4.1 n-Alkane δ^2H vs. Estimated Mean Annual δ^2H of Precipitation

Based on the findings of this study, and consistent with prior work (Sachse et al. 2012, Liu and An 2019, McFarlin et al. 2019), both gymnosperm δ^2H_{alkane} and soil δ^2H_{alkane} correlate significantly with the OIPC estimated mean annual δ^2H_{precip} over northern Washington State.

There are differences between soil and gymnosperm δ^2H_{alkane} values in part because, even though gymnosperms are the dominant plant type at many sites in this region (Pojar and Mackinnon 2014), angiosperms produce substantially more *n*-alkanes than gymnosperms do (Diefendorf et al. 2015), with some exceptions (Schlanser et al. 2022), resulting in their *n*-alkanes comprising a major component of the soil *n*-alkane reservoir even when locally outnumbered by gymnosperms (Nelson et al. 2018). The specific types of gymnosperm present at each site depend on environmental factors such as how recently the site was burned, the elevation, the proximity to the coast, the proximity of water, and MAT and MAP (Lyons 1999). This means that which specie(s), genera, or even families contribute to each gymnosperm sample varies non-systematically from site to site. Individual species or plant functional groups may contribute more alkanes to local soils than others (Diefendorf et al. 2015), and differing species-specific chain-length preferences may lead to different species contributing larger shares of *n*-alkanes at different chain lengths (Bush and McInerney 2013). This is demonstrated by a comparison of representative chromatograms: the chain-length distribution among alkanes recovered from gymnosperms and soils at the same site differs, as do the chain-length distributions of soil alkanes from different sites and gymnosperm alkanes from different sites (Supplementary Fig. 7). For instance, the gymnosperms from westside site NUG (a monospecies assemblage consisting only of western red cedar) show much higher proportions of longer-chain-length alkanes C33, C35, and even C37, than gymnosperms from the eastside site 8MI (a two-species assemblage of ponderosa pine and Douglas fir), where the dominant chain lengths are C25, C27, and C29. However, the distribution of n-alkane chain length in the soils at each of these sites differs markedly from either gymnosperm n-alkane distribution, suggesting an input of n-alkanes from another source. Note that average δ^2H_{alkane} can be biased by chain length, given that not all *n*-alkanes were abundant enough for isotopic analysis at every site. While every effort was made to accurately represent the gymnosperms present at each sampling site, not all nearby plants could always be accessed. Further, soils incorporate *n*-alkanes from many different sources: not only higher plants, but also mosses, ferns, lichens, and even bacteria, and not only trees but also grasses, shrubs, herbs, and epiphytes. The plant composition at the site may have changed during the deposition of the soil material sampled, leading to a large degree of species-averaging in the soil δ^2H_{alkane} signal. The soils may contain material from other biomes, lofted to that site by the wind (Nelson et al. 2017), introduced by slope movement, and/or washed in during storm events.

Spatial averaging would function to artificially enlarge the sampling site, increasing the potential number of species included in the soil *n*-alkane signal (but not the plant *n*-alkane signal), but also increasing the possibility that the site's estimated annual δ^2H_{precip} is not the same as the δ^2H_{precip} at the site where the soil's *n*-alkanes were originally synthesized, particularly if there are local microclimates.

Temporal averaging functions to dampen seasonal effects and short-lived changes in local δ^2H_{precip} – for instance, cold spells or droughts – in favor of longer-term trends, obscuring small-scale heterogeneities in the δ^2H_{alkane} signal and potentially decreasing noise. The amount of time-averaging present in a soil sample depends in part on the soil type, as alpine soils can be hundreds or thousands of years old, while temperate forest soils may be half that age (Trumbore 2000, Shi et al. 2020). Of the gymnosperms sampled in this study, only the larch loses and regrows its needles each year. Prior work has demonstrated that a plant's δ^2H_{alkane} value is set during the time of initial leaf flush and generally does not change thereafter (e.g., Pedentchouk et al. 2008, Tipple et al. 2013). Since the growing season varies by plant type (Harrington et al. 2016) and δ^2H_{precip} may vary strongly throughout the year, a plant's δ^2H_{alkane} value may not be representative of the mean annual δ^2H_{precip} value at that site. In a warm year, plants are likely to experience leaf flush earlier in the year than they would in a cold year, and in a dry year plants may stop growing and producing *n*-alkanes earlier than they would in a wet year, leading to further temporal variations. If the δ^2H_{alkane} value of a conifer needle is set during its initial growth, that signal may carry forward many years without being affected by later changes in local δ^2H_{precip}. The lifespan of a conifer needle depends on both the species and the local environment, particularly MAT, with needle longevity in a single species increasing in regions with colder average temperatures (Reich et al. 2014). As with soils, this could lead to greater time-averaging in samples taken from alpine sites than in lowland samples.

There appear to be strong regional differences in the relationship between gymnosperm δ^2H_{alkane} values and the estimated annual δ^2H_{precip}. The Cascades stand out as having a significantly steeper gymnosperm δ^2H_{alkane} vs δ^2H_{precip} slope than the global one (Fig. 2). The Cascades samples, which represent the majority of this data from western North America, derive from a higher latitude than all but three published gymnosperm δ^2H_{alkane} sites, primarily derive from higher elevations than most of the literature data (68 of the 87 literature sites lie below 11 of the 14 Cascades sites), and derive from a region with a strong, relatively-narrow climatic

gradient, while the majority of the literature data represent regions with much larger-geographic-scale gradients in climate (e.g., Tipple and Pagani 2013). Similarly, the climatic regime covered by the outlier study Zhang et al. (2017), in the southern-central Tibetan Plateau, is unique from other regions with published gymnosperm δ^2H_{alkane} data, primarily due to the elevation (only 6 literature sites are higher in elevation than the lowest-elevation site in Zhang et al. 2017). The high elevation may shorten the growing season, leading to an increase in δ^2H_{alkane} seasonal bias, which could flatten the gymnosperm δ^2H_{alkane} vs δ^2H_{precip} slope when compared to that of lower elevations with longer, multi-month growing seasons. The Tibetan Plateau is subject to low MAP, which could lead (1) to lower apparent fractionations in plant alkanes due to water stress, which lowers stomatal conductance (Shepherd and Griffiths 2006, Pedentchouk et al. 2008); or (2) to plants drawing upon either evaporation-dominated water sources that are enriched in ^2H relative to precipitation, giving an artificially-lower apparent fractionation when compared to the mean annual δ^2H_{precip} (Kim and Lee 2011), or water sources dominated by groundwater or glacier melt, which would lead to an insensitivity of the plant's *n*-alkanes to local modern δ^2H_{precip}. Conifers at high altitudes may experience "frost drought", whereby freezing temperatures induce water stress in leaves, leading the plants to close their stomata and limit transpiration to avoid desiccation (Mayr et al. 2006), a process observed to occur in spring (Esch and Mengel 1998b), that could lead to decreased sensitivity to δ^2H_{precip} in the plants' needles. In contrast to Zhang et al. (2017)'s study area, however, the western Cascades represent a wetter, milder climate, allowing for high stomatal conductance, which – along with the colder, more-arid conditions of the eastern Cascades - could account for the steeper relationship between δ^2H_{alkane} and δ^2H_{precip} observed in the Cascades. As the size of the Cascades dataset increases, comparison between this relationship to the east and west of the Cascade Range crest should confirm whether or not the steeper gymnosperm $\delta^2H_{alkane}/\delta^2H_{precip}$ slope in the Cascades transect is a robust feature of this mountain range.

The differences in taxonomic $\delta^2H_{alkane}/\delta^2H_{precip}$ trends between the two major extant gymnosperm families, Cupressaceae and Pinaceae, globally and in the Cascades, may be due to the families' primary water-use behavior. Isohydric plants limit transpiration and/or stomatal conductance in order to maintain a constant amount of water in their leaves, while anisohydric plants continue to transpire even when soil water content diminishes (Tardieu and Simmoneau 1998). Pinaceae tends toward isohydry, while Cupressaceae are generally anisohydric (e.g. West

et al. 2007, Meinzer et al. 2014), making members of that family more sensitive to local climate than co-occurring Pinaceae species (Voelker et al. 2018). Family is not, however, a guarantor of isohydric or anisohydric behavior in a plant, and even a single genus or species may not be internally consistent in its stomatal dynamics (Warren et al. 2003, Poulos et al. 2012, Brodribb et al. 2014, Martinez-Vilalta et al. 2014). Comparison between the Cascades data and the literature (Fig. 3b) implies that Pinaceae δ^2H_{alkane}, like Cupressaceae δ^2H_{alkane}, does reflect mean annual δ^2H_{precip}, and that the same unique setting that makes Zhang et al. (2017) (which exclusively sampled Pinaceae gymnosperms) an outlier regionally also does so taxonomically. In other words, perhaps it is not that the bulk of the family Pinaceae behaves isohydrically, but rather primarily Pinaceae in extreme high elevations like those sampled in Zhang et al. (2017), while at other published sites Pinaceae behaves similarly to Cupressaceae. Alternate explanations may include one or more other biological effects, such as differences in leaf physiology, NADPH incorporation, lipid synthesis pathway, differential responses to light intensity, or membrane permeability, among others (Sachse et al. 2012). Future study of the xylem and leaf water of sampled plants in these settings would provide insight into such effects.

4.2 Apparent Fractionation Factor (Alpha)

Fractionation factor (alpha) is used to isolate the biosynthetic portion of the apparent isotopic fractionation between the δ^2H of a plant's source water and its δ^2H_{alkane}. Because this study does not include measurements of the plant's internal waters, δ^2H_{precip} and surface water δ^2H were used as proxies for synthetic water source. The apparent fractionation factors reported here therefore have a large measure of embedded uncertainty, as they rely on either OIPC estimated mean-annual δ^2H_{precip}, which itself includes significant uncertainty due to the large spatial variability of the Cascades at scales smaller than the OIPC grid, or on the δ^2H of surface water samples, which represent an instantaneous measurement related in an uncertain way to the spatially and temporally integrated water signal recorded by the leaves. This high degree of embedded uncertainty may account for the lack of strong correlations of source water and alpha seen in both this work and for the literature gymnosperm data. Literature gymnosperm δ^2H_{alkane} exhibits the expected trend: as elevation increases (and local humidity and MAT decrease), the plants exhibit less fractionation, as evaporating leaf water, presumably, preferentially removes lighter isotopes from the plant's internal waters (Fig. 4). However, the Cascades show the

opposite trend: increasing fractionation with altitude. This may be due to the change in species composition from east to west or from low to high elevation, as the same species are not present at all sites. Furthermore, all gymnosperms present at a site were pooled, so specific species effects are obfuscated. Comparison of gymnosperm alpha by family indicates a higher correlation with altitude for Pinaceae over Cupressaceae, but only when the high-elevation Tibetan Plateau study Zhang et al. (2017) is included (Supplementary Fig. 6); however, the correlation is not statistically significant for Cupressaceae (p=0.658). It is possible that elevation effects are greater at more extreme elevations, that Cupressaceae as a family is insensitive to elevation-dependent changes when fractionating hydrogen to form n-alkanes, or that other biological effects are at play. Greater data coverage in a larger variety of biomes would help elucidate the reasons behind the trends in fractionation factor.

4.2 Isotopic Lapse Rate

The hydrogen isotopic lapse rate is the decrease in δ^2H with increasing elevation. Across the Cascades transect, gymnosperm δ^2H_{alkane} values decreased by 32‰ per km of elevation (R^2 = 0.4609, p=0.007, n=14), which is very similar to the isotopic lapse rate for published gymnosperm δ^2H_{alkane} values from the eastern United States (-32.5‰ km^{-1}; R^2 = 0.1503, p=0.002, n=59) (Supplementary Fig. 8), but larger than the lapse rate for all previously published North American gymnosperm δ^2H_{alkane} values together (-19‰ km^{-1}; R^2 = 0.082, p=0.020, n=66). Zhang et al. (2017) obtained a lapse rate of -22.8‰ km^{-1} using δ^2H_{alkane} values from gymnosperms and grasses (R^2 = 0.34, p=0.0135, n=17), which is closer to the Cascades soil *n*-alkane hydrogen isotopic lapse rate. The lack of correspondence between the Cascades gymnosperm δ^2H_{alkane} lapse rate and that for all North America is likely due to the dependence of lapse rate on air-mass sourcing: a meaningful lapse rate requires a localized area in which atmospheric moisture derives from the same or similar source(s) throughout the sampled region. The lower lapse rate observed in gymnosperm δ^2H_{alkane} in Zhang et al. (2017) is probably due to lower sensitivity to atmospheric δ^2H (see previous section), while the gymnosperms of eastern North America behave similarly to those of the Cascades because of the relatively milder climate characterizing both regions.

Soil δ^2H_{alkane} in the Cascades decreased by 22‰ per km of elevation (R^2 = 0.24, p=0.003, n=33) (Fig. 5), an isotopic lapse rate similar to the modelled OIPC δ^2H_{precip} decrease of 20‰ km^{-}

^{1} elevation across the Cascades. Data from other orogenies show similar but not identical hydrogen isotopic lapse rates, with soil *n*-alkanes demonstrating a steeper lapse rate than water samples. These include the Sierra Nevada (meteoric water δ^2H; -17‰ km^{-1}; Mulch et al. 2006); soil *n*-alkane δ^2H (-21.8‰ km^{-1}) and meteoric water and stem-water δ^2H (-18.0‰ km^{-1}) from the Southern Alps of New Zealand (Zhuang et al. 2015); the Andes of southern Ecuador (surface water δ^2H; -14‰ km^{-1}; Gebelin et al. 2021); surface water δ^2H from the Taurus Mountains (-20‰ km^{-1}) of southern Turkey and the Pontic Mountains (-19‰ km^{-1}) of northern Turkey (Schemmel et al. 2013); the Pamirs of Tajikistan (soil *n*-alkane δ^2H; -14‰ km^{-1}; Aichner et al. 2021); and the Tibetan Plateau, in north-central India (meteoric water δ^2H; -26.1‰ km^{-1}; Kumar et al. 2010), and in southern China, as measured in soil *n*-alkanes, to the north of Myanmar (-19‰ km^{-1} and -14‰ km^{-1}) and in central Tibet (-24‰ km^{-1}) (Bai et al. 2015). The variability in lapse rates arises from the variety of air masses that function as precipitation sources for these mountain ranges, as well as climatic differences such as the presence of a monsoon. However, the mountain range among these most similar to the Cascades, New Zealand's Southern Alps, has the most similar soil-alkane hydrogen isotopic lapse rate; these are a narrow coastal mountain range with a strong precipitation rain shadow and a temperate climate akin to the Cascades. Soils probably exhibit steeper lapse rates than water samples because of the different timescales over which atmospheric moisture is sampled in the water (which gives the lapse rate at the time of sampling) and in the soils (which represent a long-term temporal average, as discussed in the previous section).

The hydrogen isotopic lapse rate exhibited by the surface-water samples collected in this study is effectively zero (Fig. 5) and statistically insignificant, indicating that the δ^2H of surface waters collected at the same sites as the plant and soil samples is independent of site elevation. This also implies that (1) the surface waters sampled were not the primary water source for the sampled plants when they synthesized their leaf-wax *n*-alkanes, and (2) the water source for the sampled surface waters is at a different elevation than the elevation at which the waters were sampled and/or was precipitated during a different time of year. Bershaw et al. (2020) conducted a study of the δ^2H values of surface waters with known, restricted source areas across the Cascades (Supplementary Fig. 9) and determined that the isotopic lapse rate was -6.7‰ km^{-1} elevation, close to an order of magnitude less than the *n*-alkane lapse rates derived in this study and others across similar orogenies; this anomalously-low hydrogen isotopic lapse rate is due to

the strong influence of evaporative ^{2}H-enrichment on their highest-elevation samples, particularly to the east of the Cascade crest, where it is more arid.

The correlation of surface water δ^2H with mean annual δ^2H_{precip} is noisy over the Cascades (Fig. 6a) and globally (Fig. 6b) due in part to sourcing issues: surface waters may come from groundwater, which has been out of contact with local precipitation and therefore will not reflect local δ^2H_{precip}; from ice- and snow-melt, which is likely to differ in δ^2H from local δ^2H_{precip}, as snow preferentially reflects the δ^2H of the upper atmosphere and of the colder season when it was formed (Mook et al. 1974); and/or from a long distance away, such that it will reflect the δ^2H_{precip} of a different location than the sampling site. Likewise, the δ^2H value of local surface waters may vary strongly throughout the year. For instance, the spring snowmelt might cause an influx of water with much lower δ^2H values than the yearly average, reflecting the δ^2H of snow that precipitated during winter; source tributaries for a river or stream might be removed as they dry up with the progression of summer and/or changing drainages; or lakes might switch from being precipitation-dominated to evaporation-dominated as the summer becomes drier. While seasonal bias is nominally accounted for in the OIPC reanalysis products to which the Cascades data are compared, heavier rainfall during the spring (https://psl.noaa.gov/cgi-bin/data/usstation/state.pl?lane=scroll&state=WA) might lead to a stronger bias in surface waters towards the δ^2H_{precip} of those months than is represented by interpolated data.

4.3 Covariation of Environmental Variables

The effects of temperature on δ^2H_{precip} are well-documented (e.g., Dansgaard 1964, Mook 2001), with colder air promoting condensation of ^{2}H-enriched precipitation, leaving the residual vapor ^{2}H-depleted through Rayleigh distillation. Temperature and elevation are closely linked, with a mean atmospheric temperature lapse rate in the Cascade Mountains of -4 to -5 °C km^{-1} (Minder et al., 2010) (Fig. 1d). In the Cascades, elevation and δ^2H_{precip} covary (Supplementary Fig. 2). Further complicating matters, elevation and MAT have strong effects on plant biology and soil processes. Alpine soils, for instance, tend to be considerably older than lowland soils, sometimes by an order of magnitude (Trumbore 2000, Shi et al. 2020), as they develop much more slowly; the alpine growing season tends to begin later in the year (due to persistent snow cover) and to be of shorter duration than the lowland growing season (Berdanier and Klein 2011, Barnard et al. 2017); and, due to the harsher climate, alpine gymnosperms tend to grow much more slowly than

their lowland counterparts, with members of the same species expressing as a tree at low elevations and as a sprawling shrub at high elevations despite the two plants being the same age (e.g., Lyons 1999). A shorter, later growing season could bias a plant's δ^2H_{alkane} towards precipitation from just a few months out of the year, introducing different patterns of seasonality than the regional average. Finally, a smaller, slower-growing tree retains its needles longer than a larger, faster-growing member of the same species (Reich et al. 2014), thus decreasing the year-to-year climate sensitivity of the plant's leaf *n*-alkanes. In the Cascades, gymnosperm δ^2H_{alkane} values appear to be more sensitive to elevation and/or MAT than the more temporally, spatially, and biologically diverse soil δ^2H_{alkane} values (Supplementary Fig. 3).

Previous work has noted a correlation between latitude and the δ^2H_{alkane} value of plants and soils (Tipple and Pagani 2013), due to the global relationship between MAT and latitude and the latitude effect on δ^2H_{precip}, which functions to decrease δ^2H_{precip} as distance from the equator increases (Yurtsever 1975). On a global scale, the effects of elevation on MAT are minor when compared to the effects of latitude (Supplementary Fig. 5); however, on a local scale – for instance, across a single orogeny like the Cascades – MAT may become primarily a function of altitude, such as seen in Zhang et al. (2017).

In the Cascades, δ^2H_{alkane} values are much more influenced by DAT (or longitude) than by latitude, as the climate in this region changes far more drastically from east to west (zonally) than from north to south (meridionally). MAP varies strongly - but not monotonically - with DAT (Fig. 1c); it is equally low at the westernmost and easternmost ends of the transect. This trend leads to rainout of increasingly ^2H-depleted water from west to east as air masses move across the mountains (Roe 2005, Roe and Baker 2006). This can be seen in the surface water δ^2H values (Fig. 6a) and in the estimated annual δ^2H_{precip} values (Supplementary Fig. 2a) that become increasingly negative from west to east along the transect. This effect is also visible in Bershaw et al. (2020), where the δ^2H values of water from small-catchment streams across the northern half of Washington State exhibit a stronger negative correlation with longitude (from west to east, conceptually equivalent to DAT in the Cascade alkane dataset) ($R^2 = 0.694$) than with altitude ($R^2 = 0.026$). Locally, the greatest control on δ^2H in *n*-alkanes and in both meteoric and surface waters seems to be the orogenic rain shadow effect, which far outweighs altitude effects.

When the difference between δ^2H_{precip} and δ^2H_{alkane} from the dataset average is compared between west and east, a distinct difference is observed: to the west, the average δ^2H is more

than the transect average, while to the east the average δ^2H is less than the transect average, indicating heavier-than-average isotopes to the west (windward) of the Cascade crest and lighter-than-average isotopes to the east (leeward) of the Cascade crest (Fig. 7). The δ^2H_{precip} difference is negative at the highest elevation sites west of the crest likely due to the fact that the highest mean annual rainfall, and the minimum δ^2H_{precip}, occurs slightly windward of the mountain crest (Roe and Baker 2006). The trends in the average δ^2H_{alkane} of gymnosperms and soils east and west of the Cascades crest supports the use of δ^2H_{alkane} as a tool for determining the presence of a mountain range in the rock record. By comparing δ^2H_{alkane} values between the west and east sides of the modern mountain range through time, an increase in the difference from average on either side should indicate a growing orographic rainshadow.

4.4 Reconstructing Rainshadow Strength in the Geologic Past: Proof-of-Concept

A promising application of δ^2H_{alkane} measurements in mountainous regions is to infer the strength of the orogenic rainshadow over time to assess orographic history (Hren et al. 2010, Zhuang et al. 2014, Burrington 2015, Massa et al. 2021, Yanuskiewicz et al. 2022). Using δ^2H_{alkane} from sedimentary rocks to infer the strength of a rainshadow in the geologic past requires some additional considerations beyond those needed for soils and plants. Organic content from sedimentary rock samples and paleosols may differ from soil samples in that they may have undergone more diagenetic alteration, but will otherwise likely be susceptible to the same issues as soils: time-averaging, species-averaging, and spatial averaging (Bush et al. 2002, Kowalewski and Bambach 2008). One caveat is that (non-paleosol) sedimentary rocks may not derive from soils directly, but are likely to be lacustrine, fluvial, or marine in origin; this will present sourcing issues, as the constituent *n*-alkanes may have been brought to the site from some unknown distance. Nevertheless, the two rock samples analyzed as a simple proof-of-concept in this study have reasonably similar δ^2H_{alkane} values to modern soils (Fig. 8). This implies that local *n*-alkanes can be recovered from local marine sedimentary rocks, opening up the possibility of applying this technique to the Cascades and ultimately to other mountain ranges that produce a marked rain shadow.

5. Implications and Conclusions

Gymnosperm and soil δ^2H_{alkane} values are significantly correlated with δ^2H_{precip} in northern Washington State using ordinary least-squares regression ($p=2^{-8}$ to 0.0001 for soils, p=0.00002 to 0.0003 for gymnosperms). Globally, while gymnosperm δ^2H_{alkane} does reflect δ^2H_{precip}, there are strong regional differences in this relationship, particularly in the high-elevation southern Tibetan Plateau, which appears as an outlier relative to all other published sites. While a global calibration may be possible with more gymnosperm δ^2H_{alkane} data, the currently available data, which show large differences in the gymnosperm $\delta^2H_{alkane}/\delta^2H_{precip}$ relationship between southern Tibet, the rest of Asia, and the eastern and western United States, imply that regional calibrations may be more appropriate when attempting to infer past δ^2H_{precip} values from sedimentary δ^2H_{alkane} values. Unless the original environment was especially harsh, however, the published data suggest that the taxonomic origin of an *n*-alkane is not crucial to the interpretation of the gymnosperm δ^2H_{alkane} signal, with the two major conifer families (Cupressaceae and Pinaceae) exhibiting similar δ^2H_{alkane} trends as a function of δ^2H_{precip} when not grown in extreme climates.

The Cascades data suggest that δ^2H_{alkane} of both soils and plants could provide a good proxy for cumulative amount of rainout, in the form of a correlation with DAT on a transect corresponding to the direction of a strong regional rain shadow. The presence or absence of such a rain shadow in the past - and, by extension, of a mountain range such as the Cascades - could be inferred from the presence or absence of a strong correlation between sedimentary δ^2H_{alkane} and DAT (for an east-west transect, in this region). Finally, if the proxy is being used to detect a particular climatic feature in the past, such as an orographic rainshadow like that produced by the modern Cascades, an important consideration is that this study involves a very strong, abrupt rainshadow, which would tend to accentuate δ^2H changes due to rainout. A less-pronounced climate gradient – for instance, the rainshadow produced by a shorter or lower-elevation mountain belt - might not be as prominent in the δ^2H_{alkane} data.

Acknowledgements

Funding for this work was provided by the Quaternary Research Center, the University of Washington Royalty Research Fund (grant number 127283), and the University of Washington Earth and Space Sciences Department. Samples from the North Cascades National Park were collected under permits NCCO-2018-SCI-0026 and NCCO-2019-SCI-0021. Field assistance was

provided by Tracy Sisley, Anthony Poon, Junko Matsuda and Steven Newman, the Vallins family, and the Kuester family.

Figures

Fig. 1. Overview of sampling area. (a) Map of Washington State, USA, with mean annual precipitation, showing the Cascade rainshadow. Black box indicates sampling area. (b) Inset map showing all samples collected and analyzed; grayscale indicates elevation, with white being highest and black lowest; colors on inset map denote the year the sample was collected. Grey boxes denote 18 sampling sectors, designated to ensure sufficient E-W data coverage; these were obtained by dividing the sampling area in 18 equal sections. Rock samples were collected proximal to the westernmost 2017 sample and plot coincident with that data point on the map. (c) OIPC δ^2H_{precip} at sampling sites and mean annual precipitation (MAP) of each sampling sector vs. distance along transect from west to east (DAT). To illustrate spatial variability of MAP across the North Cascades, MAP at 25 evenly-spaced E-W transects across the sampling area outlined in *(b)* is shown in pale blue; dark blue is a 10-point moving average of this MAP data. (d) Mean elevation and mean annual temperature (MAT) of sample sites and sampling area vs. DAT. Pale yellow indicates elevation profiles along the 25 transects defined in *(c)*, with a 10-point moving average of such shown in gold. See Supplement for more information on sampling sectors *(b)*, MAP transects *(c),* and MAT transects *(d)*.

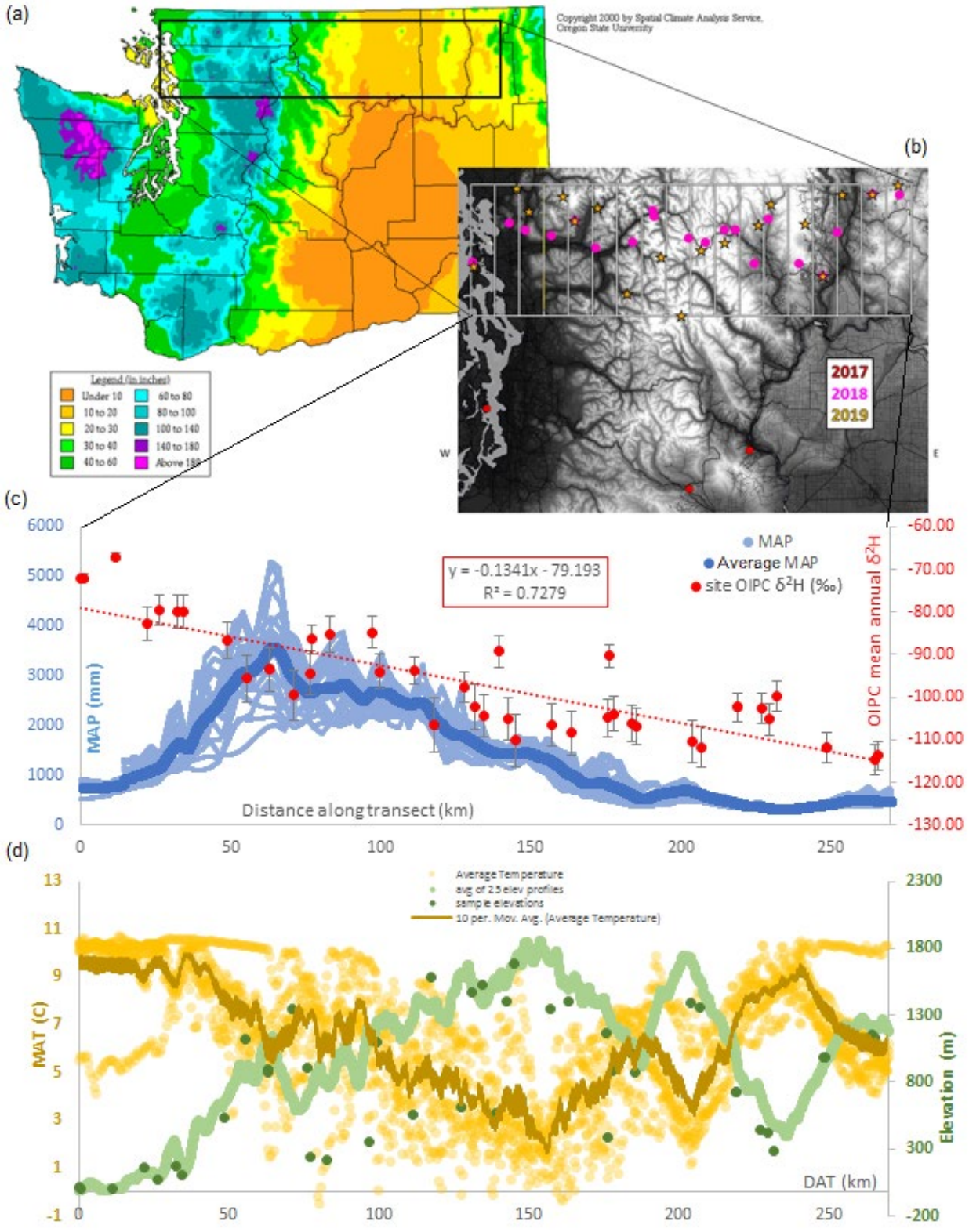
(a)
Copyright 2000 by Spatial Climate Analysis Service, Oregon State University
Legend (in inches)
Under 10
10 to 20
20 to 30
30 to 40
40 to 60
60 to 80
80 to 100
100 to 140
140 to 180
Above 180
(b)
2017
2018
2019
W
E
(c)
y = -0.1341x - 79.193
R² = 0.7279
MAP
Average MAP
site OIPC δ²H (‰)
MAP (mm)
OIPC mean annual δ²H
Distance along transect (km)
(d)
Average Temperature
avg of 25 elev profiles
sample elevations
10 per. Mov. Avg. (Average Temperature)
MAT (C)
Elevation (m)
DAT (km)

Fig. 2. OIPC δ^2H_{precip} vs. nC29-alkane δ^2H, with least-squares lines of best fit, for all Cascades sites analyzed, compared to published data. Published soil data (open small blue circles, thin solid blue line; y = 1.0088x - 112.09, R^2 = 0.7398, p<0.001, n = 446) are taken from Ladd et al. (2021), a global compilation of nC29-alkane δ^2H from soils and other sediments. Published gymnosperms (open medium-sized green triangles, thin dashed green line; y = 0.5879x - 126.48, R^2 = 0.4295, p<0.001, n = 87) exclude Zhang et al. (2017), shown as light-grey small open triangles. Cascades gymnosperms are shown as large solid dark-green triangles (thick dashed dark-green line; y = 1.8305x - 11.611, R^2 = 0.876, p<0.001, n = 14) and Cascades soils as solid brown circles (thick solid brown line; y = 1.1469x - 99.572, R^2 = 0.5885, p<0.001, n = 33). Y-error bars indicate standard deviation, and are included for all data from this study and for all published data where they were reported. Error bars are smaller than the data point in some instances. X-error bars are obtained from the OIPC (Bowen and Revenaugh 2003, Bowen 2017). See Supplementary Table 9 for sources and citations for gymnosperm data.

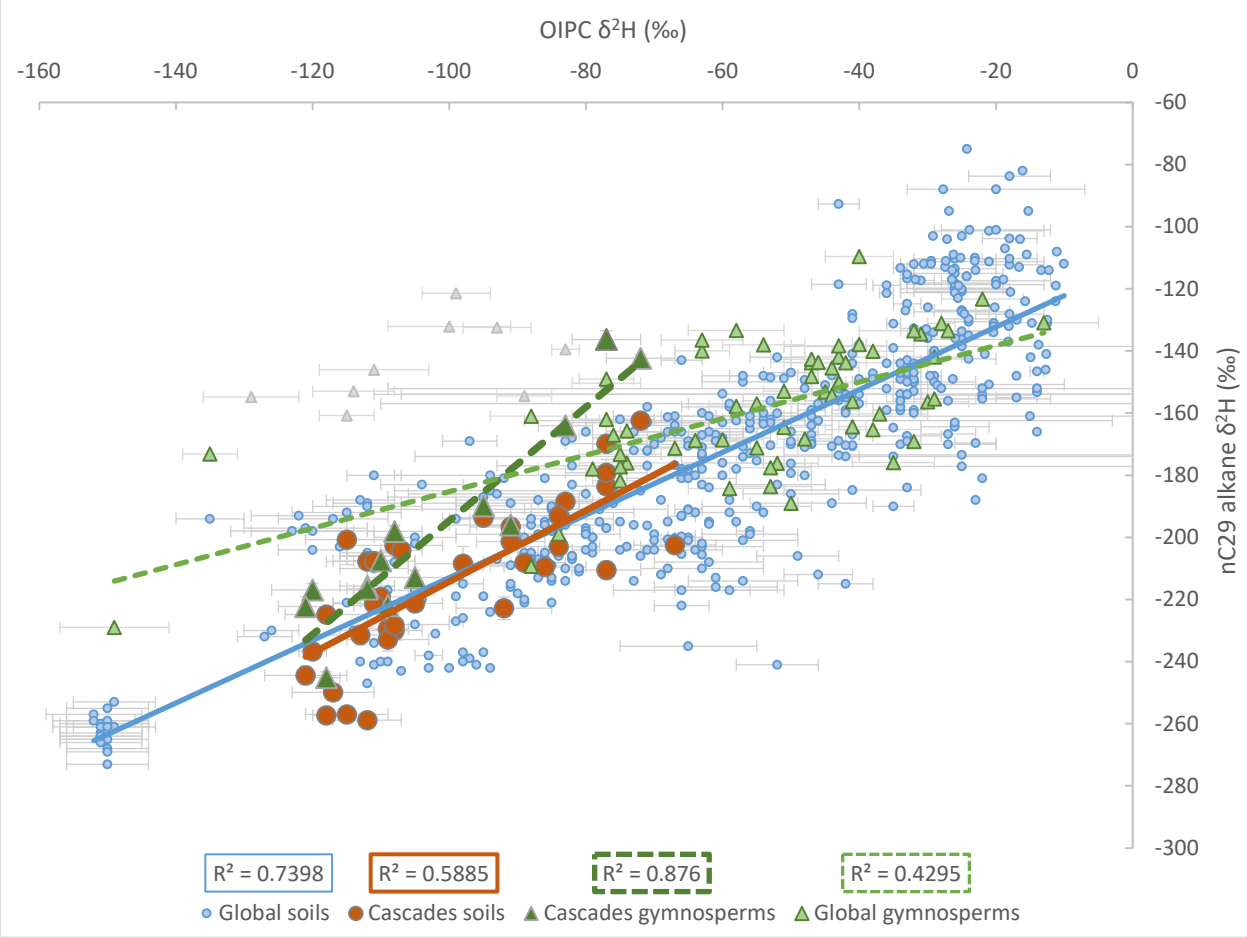

Fig. 3a. Regional differences in the relationship between gymnosperm δ^2H_{alkane} and OIPC δ^2H_{precip}, with least-squares lines of best fit. Where multiple measurements were taken at the same site, δ^2H_{alkane} values have been averaged over both time and species, so as to prevent site duplication. "East US" (yellow circles, long-dashed line; y = 0.698x - 119.11, R^2 = 0.3399, p<0.001, n=59) includes published sites spanning the east coast of North America from Maine to Florida; the westernmost sites are from Ohio, Kentucky, and Alabama. "West US" (green triangles, short-dashed line; y = 0.932x - 100.91, R^2 = 0.6421, p<0.001, n=21) includes the Cascades of Washington (this study), as well as published data from Oregon, California, and Alaska. "Asia" (red diamonds, dot-dashed line; y = 1.3035x - 67.854, R^2 = 0.5955, p=0.014, n=8) excludes Zhang et al. (2017), shown separately (blue squares, dotted line; y = 0.207x - 130.2, R^2 = 0.1634, p=0.2, n=11) and includes sites in China and Japan. Y-error bars represent standard deviation, and are included for all data from this study and for all published data where they were reported; X-error bars were obtained from the OIPC (Bowen and Revenaugh 2003, Bowen 2017). No regression is provided for Europe as gymnosperm δ^2H_{alkane} data have been published for only two sites in that region (Sweden and Switzerland). See Supplementary Table 9 for more information.

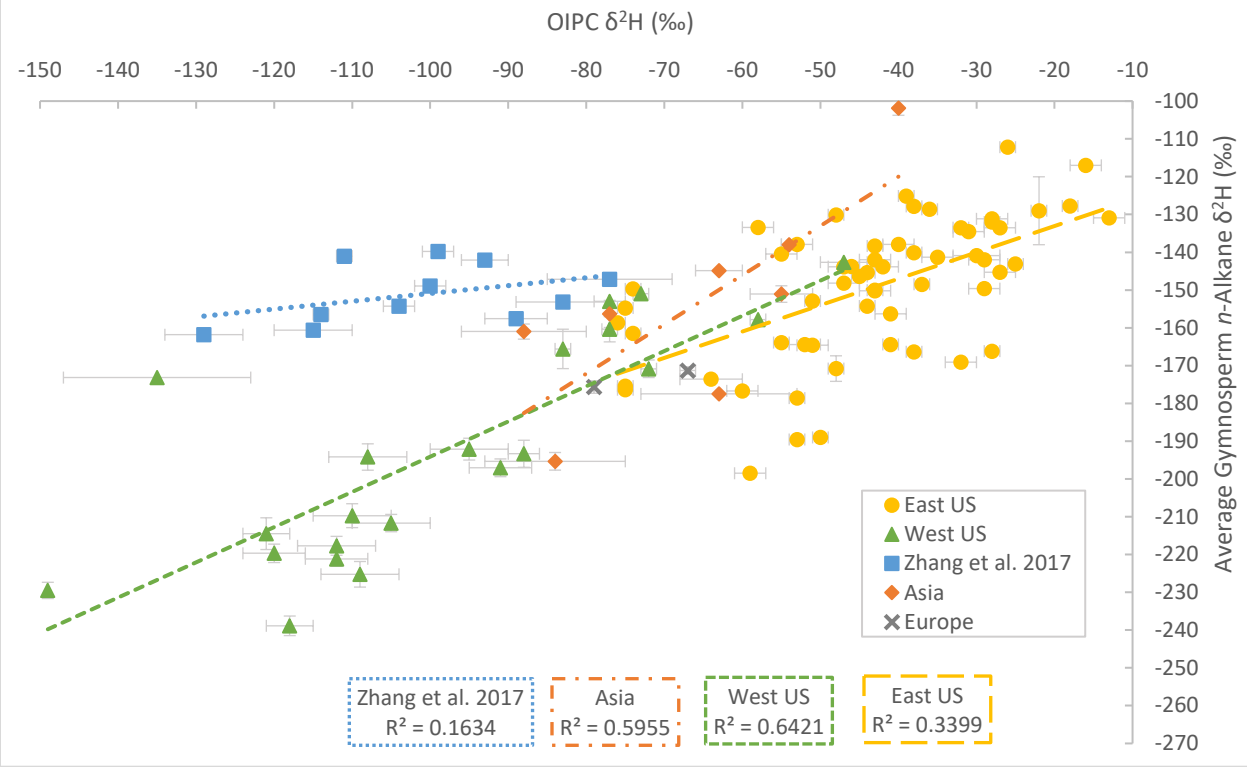

Fig. 3b. Differences in the relationship between gymnosperm average δ^2H_{alkane} and OIPC δ^2H_{precip} for different gymnosperm families, with least-squares lines of best fit. Cupressaceae is shown as green circles (dashed line; y = 0.4341x - 120.98, R^2 = 0.3216, p<0.001, n=55), Pinaceae as blue diamonds (dotted line; y = 0.6478x - 133.64, R^2 = 0.5309, p<0.001, n=45), and other families as x-marks. Data from the Cascades (this study) have darker data points with black borders. Where multiple measurements were taken at the same site, δ^2H_{alkane} values have been averaged over time and species but not by genus. Only Cascades data that represented gymnosperm δ^2H_{alkane} measurements from a single family were included. Zhang et al. (2017) (red triangles, dot-dashed line; y = 0.207x - 130.2, R^2 = 0.1634, p=0.2, n=11) exclusively contains data from Pinaceae. Y-error bars represent standard deviation and are included for all data from this study and for all published data where they were reported. X-error bars are from the OIPC output (Bowen and Revenaugh 2003, Bowen 2017). Regressions are not shown for families with less than five data points.

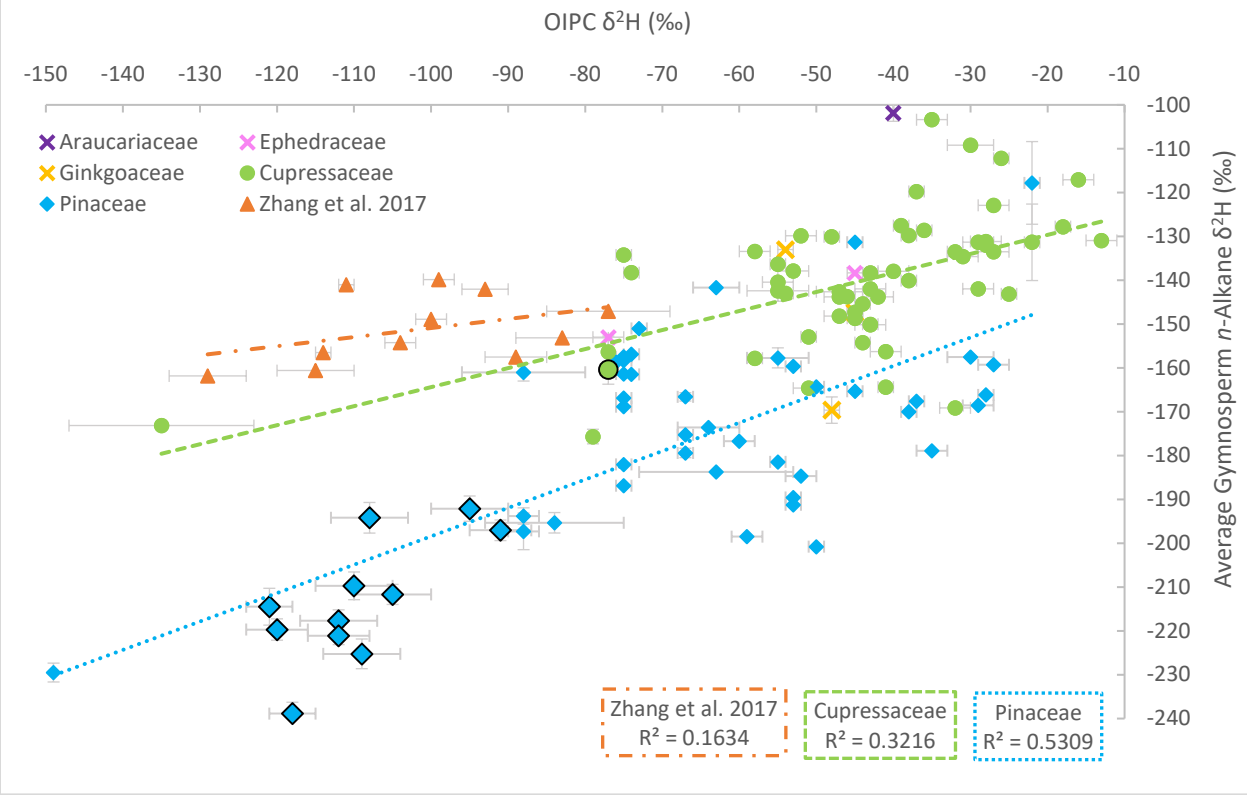

Fig. 4. Apparent fractionation factor vs. elevation, for gymnosperm nC29 δ^2H_{alkane} in the Cascades and the published literature, with best-fit ordinary least-squares regression trendlines. Two alphas were calculated for each dataset: a primary alpha, denoted by a filled symbol and a heavy-weight trendline, calculated versus OIPC estimated mean annual δ^2H_{precip}; and a "wtr" alpha, denoted by a hollow symbol and a light-weight trendline, calculated versus surface water δ^2H. Cascades data are denoted by circles and a dotted line; all literature data by triangles and a solid line; and the literature data excluding Zhang et al. (2017) by diamonds and a dashed line. Trendline statistics: Cascades gymnosperms vs. OIPC (orange heavy-dotted line): y = -3E-05x + 0.9186, R^2 = 0.4528, p=0.008, n=14; Cascades gymnosperms vs. water (yellow light-dotted line): y = -4E-05x + 0.9469, R^2 = 0.6299, p=0.059, n=6; literature gymnosperms vs. OIPC (blue heavy solid line): y = 2E-05x + 0.8846, R^2 = 0.4984, p<0.001, n=72; literature gymnosperms vs. water (red light solid line): y = 2E-05x + 0.8694, R^2 = 0.6232, p<0.001, n=26; literature (without Zhang et al. 2017) vs. OIPC (purple heavy-dashed

line): y = 6E-06x + 0.8874, R^2 = 0.0507, p=0.078, n=62; literature (without Zhang et al. 2017) vs. water (green light-dashed line): y = 9E-06x + 0.8743, R^2 = 0.1947, p=0.087, n=16.

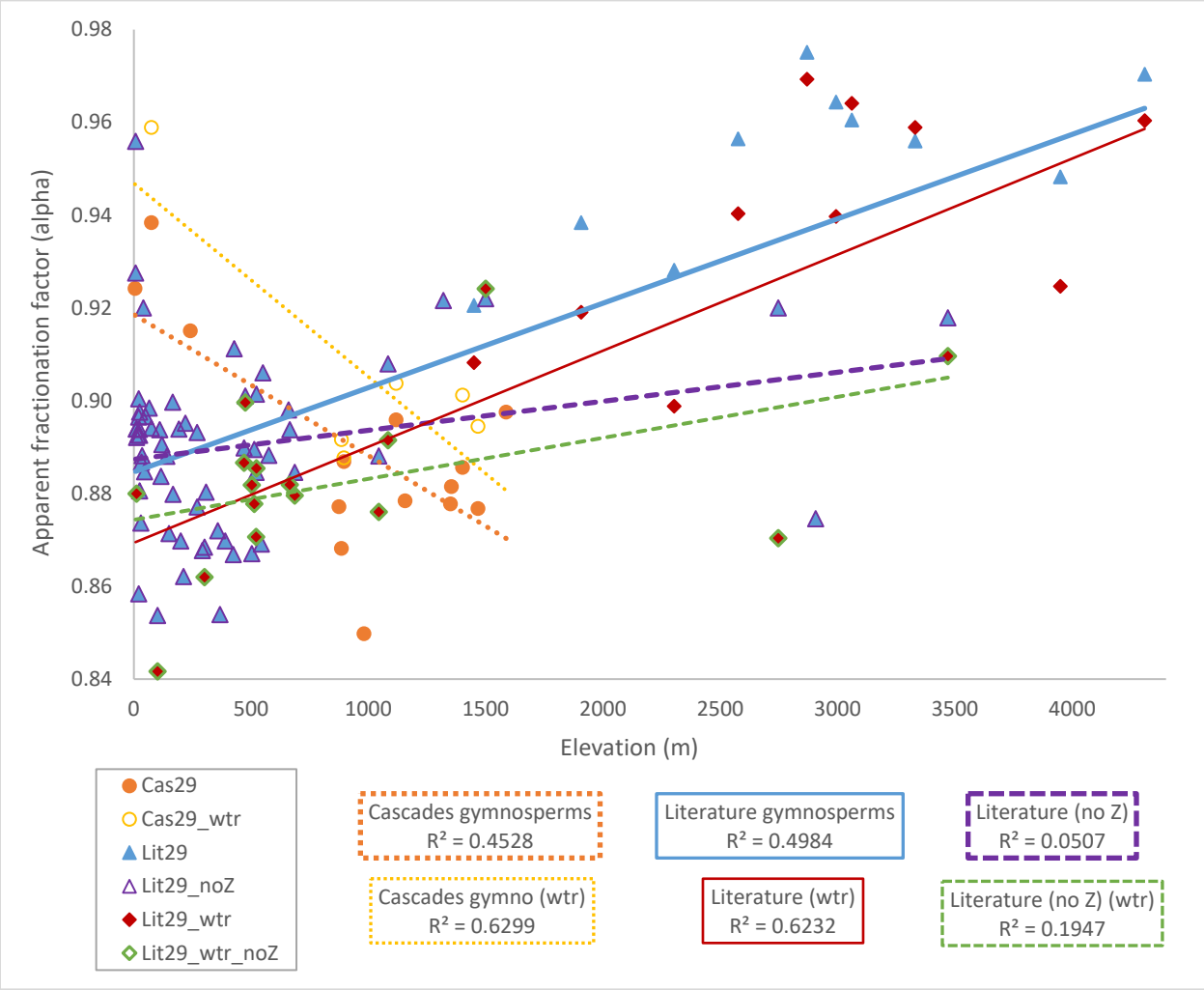

Fig. 5. OIPC δ^2H_{precip} lapse rate vs. δ^2H_{alkane} lapse rate and surface water δ^2H across transect. δ^2H_{alkane} values are given as the average of all chain lengths. There is no significant correlation between surface water δ^2H and elevation. OIPC data: red squares, small-dotted line (y = -0.0199x - 81.091, R^2 = 0.6522, p<0.001); surface water: blue triangles, dashed line (y = -0.0004x - 109.82, R^2 = 0.0002, p=0.963, n=12); gymnosperms: green diamonds, large-dotted line (y = -0.0313x - 172.8, R^2 = 0.4609, p=0.007, n=14); soils: brown circles, dot-dashed line (y = -0.0218x - 189.49, R^2 = 0.24, p=0.003, n=33).

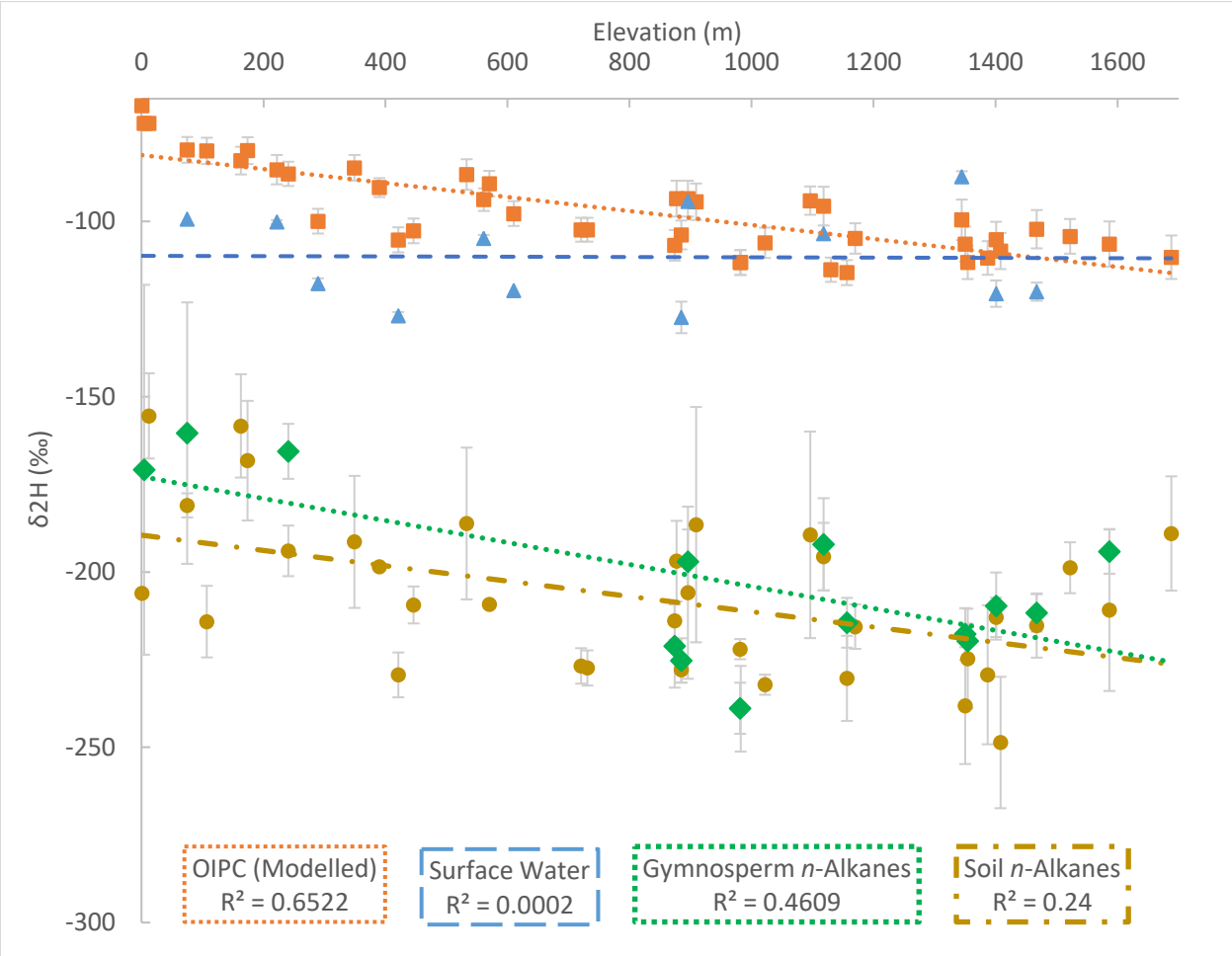

Fig. 6a. Surface water δ2H vs. distance along transect (DAT) (blue circles, dashed line; y = -0.1643x - 90.282, R^2 = 0.6567, p=0.001, n = 12) and vs. OIPC $\delta 2H_{precip}$ (red triangles, dotted line; y = 1.0898x - 4.6626, R^2 = 0.4103, p=0.025, n = 12) across the Cascades, with least-squares lines of best fit, for all sites analyzed. Y-error bars (standard deviation) are included for all data points from this study with more than one measurement. The transect begins at a longitude of 122.7 degrees west (the westernmost sample, Bowman) and ends at 119 degrees west (the easternmost sample, BIT); DAT is measured from west to east.

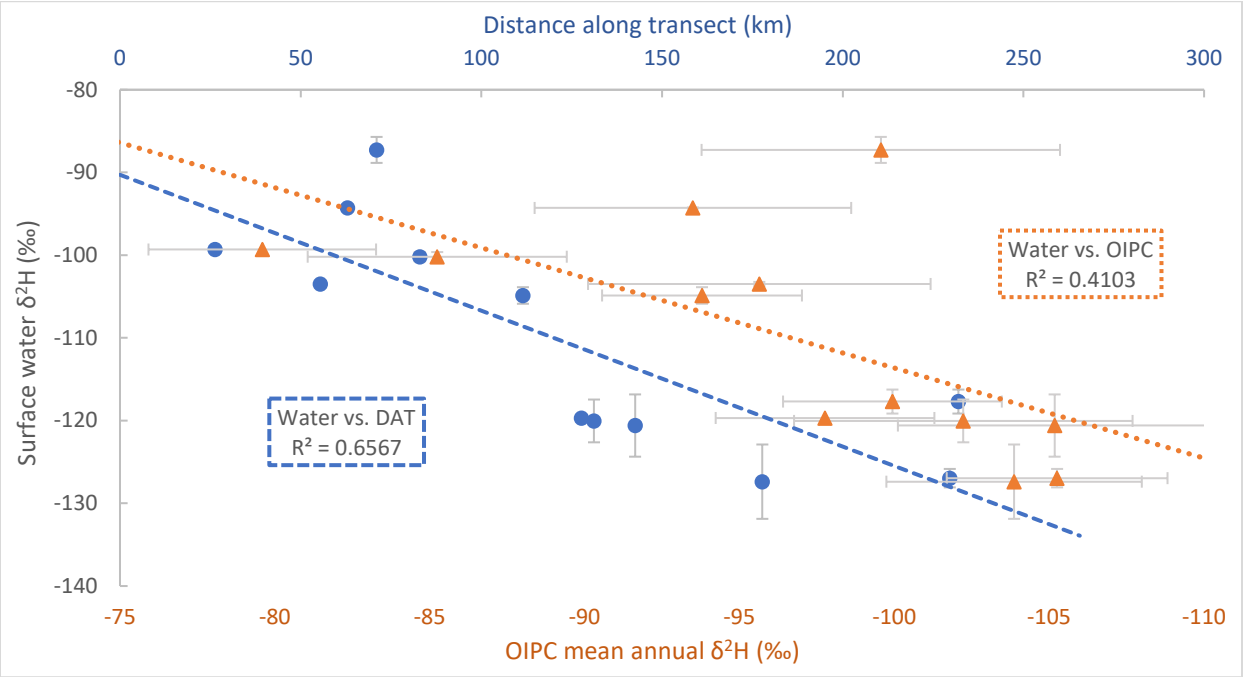

Fig. 6b. Published surface water δ^2H vs. OIPC δ^2H_{precip}, from sites where gymnosperm δ^2H_{alkane} has been published, with least-squares lines of best fit, including and excluding this study and/or Zhang et al. (2017). "C" stands for Cascades; "Z" stands for Zhang et al. (2017); "lit" denotes other published data. Trendlines are shown for all literature sites (solid blue line; $y = 0.8728x + 0.979$, $R^2 = 0.7675$, $p<0.001$, $n=33$), all literature sites except those from Zhang et al. (2017) (red dot-dashed line; $y = 0.8304x - 2.2942$, $R^2 = 0.6129$, $p=0.061$, $n=22$), all literature sites and all Cascades sites taken as a single dataset (green dotted line; $y = 1.0002x + 6.8693$, $R^2 = 0.7496$, $p<0.001$, $n=39$), and literature sites + Cascades sites excluding Zhang et al. (2017)'s sites (yellow dashed line; $y = 1.1669x + 15.093$, $R^2 = 0.7872$, $p<0.001$, $n=27$). Where multiple measurements were taken at the same site, δ^2H values have been averaged over time, so as to prevent site duplication. Y-error bars (indicating standard deviation) are included for all data from this study and for all published data where they were reported; X-error bars are taken from OIPC results (Bowen and Revenaugh 2003, Bowen 2017).

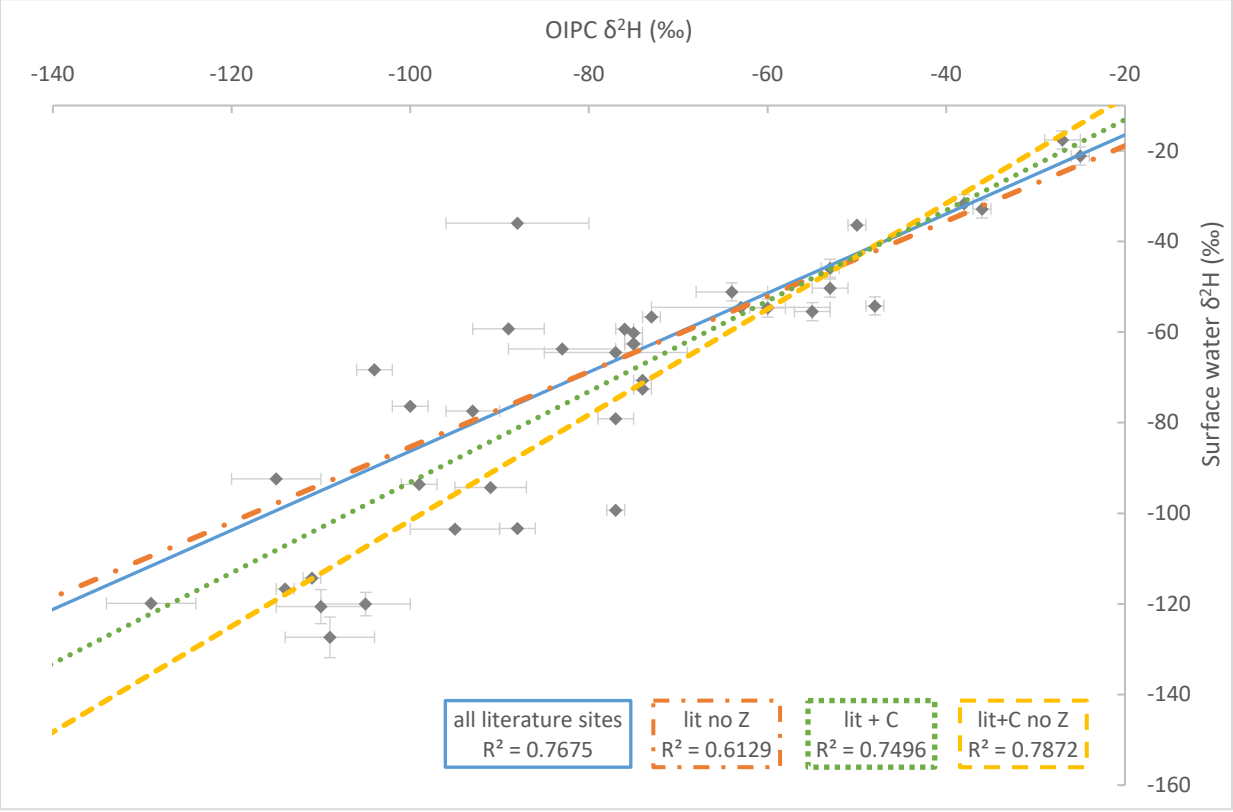

Fig. 7. Comparison of the difference in elevation-binned δ^2H_{precip} and soil and gymnosperm δ^2H_{alkane} averages on the east and west sides of the Cascade crest from the full-dataset average δ^2H_{alkane}, soil δ^2H_{alkane}, and gymnosperm δ^2H_{alkane}. OIPC modelled δ^2H_{precip}: blue bar with horizontal lines. Soil δ^2H_{alkane}: orange bar with diagonal lines. Gymnosperm δ^2H_{alkane}: solid green bar. Data used to create this graph, including averages, differences, and sample *n*, may be found in Table S13.

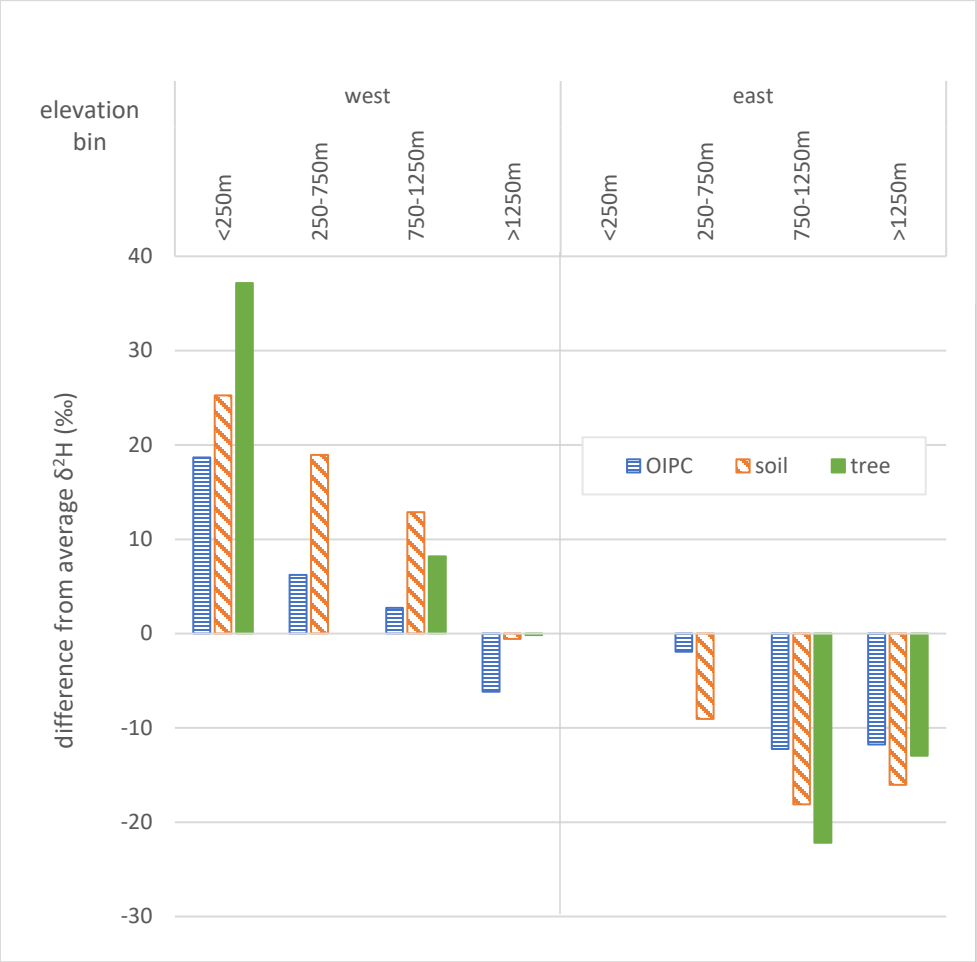

Fig. 8. OIPC mean annual δ^2H_{precip} vs. average δ^2H_{alkane}, with least-squares lines of best fit, for modern Cascades soils and gymnosperms, compared to two rock samples (Oligocene and Miocene) collected from Bainbridge Island, Washington, near one of the soil samples (BHM). Rock samples are shown as red squares (n=2) and overlap each other. The OIPC δ^2H_{precip} values associated with the rock samples are those of the modern-day sites where the rock samples were collected and do not necessarily reflect the actual δ^2H_{precip} at the time the rocks' constituent sediments were deposited. Gymnosperms are shown as green triangles (dashed line; $y = 1.6331x - 40.254$, $R^2 = 0.7681$, $p<0.001$, $n=14$) and soils as brown circles (dotted line; $y = 1.2654x - 85.135$, $R^2 = 0.5147$, $p<0.001$, $n=33$). The average δ^2H_{alkane} shown is the simple average of δ^2H values across all *n*-alkane chain lengths, referred to in the text and in Supplementary Table 6 as the type-ii average (see Supplementary Table 6).

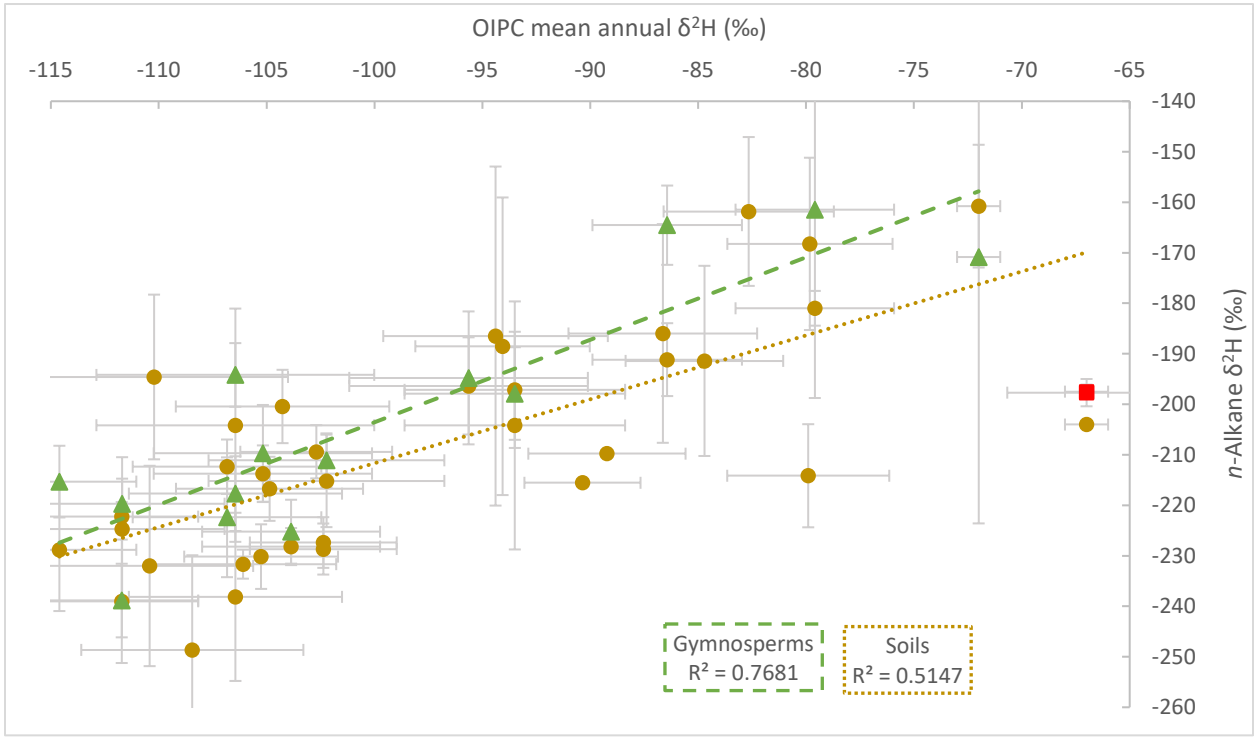

Bibliography

Aichner, B., Herzschuh, U., Wilkes, H., Vieth, A., Böhner, J., 2010. δD values of *n*-alkanes in Tibetan lake sediments and aquatic macrophytes – A surface sediment study and application to a 16ka record from Lake Koucha. Organic Geochemistry 41, 779–790.

Aichner, B., Rajabov, N., Shodmonov, M., Mętrak, M., Suska-Malawska, M., Strecker, M., Sachse, D., 2021. Local effects on soil leaf wax hydrogen isotopes along a west to east transect through the Pamirs, Tajikistan. Organic Geochemistry 160, 104272.

Allan, J., Douglas, A.G., 1977. Variations in the content and distribution of *n*-alkanes in a series of carboniferous vitrinites and sporinites of bituminous rank. Geochimica et Cosmochimica Acta 41, 1223–1230.

Bai, Y., Fang, X., Gleixner, G., Mügler, I., 2011. Effect of precipitation regime on δD values of soil *n*-alkanes from elevation gradients – Implications for the study of paleo-elevation. Organic Geochemistry 42, 838–845.

Bai, Y., Fang, X., Jia, G., Sun, J., Wen, R., Ye, Y., 2015. Different altitude effect of leaf wax n -alkane δD values in surface soils along two vapor transport pathways, southeastern Tibetan Plateau. Geochimica et Cosmochimica Acta 170, 94–107.

Barnard, D.M., Barnard, H.R., Molotch, N.P., 2017. Topoclimate effects on growing season length and montane conifer growth in complex terrain. Environmental Research Letters 12, 1–9.

Berdanier, A.B., Klein, J.A., 2011. Growing Season Length and Soil Moisture Interactively Constrain High Elevation Aboveground Net Primary Production. Ecosystems 14, 963–974.

Bershaw, J., Hansen, D.D., Schauer, A.J., 2020. Deuterium excess and 17O-excess variability in meteoric water across the Pacific Northwest, USA. Tellus B: Chemical and Physical Meteorology 72, 1–17.

Bi, X., Sheng, G., Liu, X., Li, C., Fu, J., 2005. Molecular and carbon and hydrogen isotopic composition of *n*-alkanes in plant leaf waxes. Organic Geochemistry 36, 1405–1417.

Bowen, G. J. (2017). The Online Isotopes in Precipitation Calculator, version 3.1. http://www.waterisotopes.org.

Bowen, G.J., Revenaugh, J., 2003. Interpolating the isotopic composition of modern meteoric precipitation. Water Resources Research 39, 1–13.

Brodribb, T.J., McAdam, S.A.M., Jordan, G.J., Martins, S.C.V., 2014. Conifer species adapt to low-rainfall climates by following one of two divergent pathways. Proceedings of the National Academy of Sciences 111, 14489–14493.

Buggle, B., 2011. Reconstruction of the Late and Mid-Pleistocene climate and landscape history in SE-Central Europe: A paleopedological and geochemical multi-proxy approach in loess-paleosol studies (Doctoral Thesis). Universitat Bayreuth, Bayreuth.

Burrington, P., 2015. How to be a Prehistoric Weatherman: Using *n*-alkanes as a Proxy for Holocene Climate and Hydrology, Southwest South Island, New Zealand (Masters of Science). University of Otago, Dunedin, New Zealand.

Bush, A.M., Powell, M.G., Arnold, W.S., Bert, T.M., Daley, G.M., 2002. Time-Averaging, Evolution, and Morphologic Variation. Paleobiology 28, 9–25.

Bush, R.T., McInerney, F.A., 2013. Leaf wax *n*-alkane distributions in and across modern plants: Implications for paleoecology and chemotaxonomy. Geochimica et Cosmochimica Acta 117, 161–179.

Collins, J.A., Schefuß, E., Mulitza, S., Prange, M., Werner, M., Tharammal, T., Paul, A., Wefer, G., 2013. Estimating the hydrogen isotopic composition of past precipitation using leaf-waxes from western Africa. Quaternary Science Reviews 65, 88–101.

Dansgaard, W., 1964. Stable isotopes in precipitation. Tellus 16, 436–468.

Diefendorf, A.F., Leslie, A.B., Wing, S.L., 2015. Leaf wax composition and carbon isotopes vary among major conifer groups. Geochimica et Cosmochimica Acta 170, 145–156.

Doman, C.E., 2015. Stable isotope and lipid signatures of plants across a climate gradient: Implications for biomarker-based plaeoclimate reconstructions (MS). Pennsylvania State University.

Douglas, P.M.J., Pagani, M., Brenner, M., Hodell, D.A., Curtis, J.H., 2012. Aridity and vegetation composition are important determinants of leaf-wax δD values in southeastern Mexico and Central America. Geochimica et Cosmochimica Acta 97, 24–45.

Ernst, N., Peterse, F., Breitenbach, S.F.M., Syiemlieh, H.J., Eglinton, T.I., 2013. Biomarkers record environmental changes along an altitudinal transect in the wettest place on Earth. Organic Geochemistry 60, 93–99.

Esch, A., Mengel, K., 1998. Combined effects of acid mist and frost on the water status of young spruce trees (Picea abies). Chemosphere 36, 645–650.

Feakins, S.J., Bentley, L.P., Salinas, N., Shenkin, A., Blonder, B., Goldsmith, G.R., Ponton, C., Arvin, L.J., Wu, M.S., Peters, T., West, A.J., Martin, R.E., Enquist, B.J., Asner, G.P., Malhi, Y., 2016. Plant leaf wax biomarkers capture gradients in hydrogen isotopes of precipitation from the Andes and Amazon. Geochimica et Cosmochimica Acta 182, 155–172.

Feakins, S.J., Sessions, A.L., 2010. Controls on the D/H ratios of plant leaf waxes in an arid ecosystem. Geochimica et Cosmochimica Acta 74, 2128–2141.

Feakins, S.J., Wu, M.S., Ponton, C., Galy, V., West, A.J., 2018. Dual isotope evidence for sedimentary integration of plant wax biomarkers across an Andes-Amazon elevation transect. Geochimica et Cosmochimica Acta 242, 64–81.

Gébelin, A., Witt, C., Radkiewicz, M., Mulch, A., 2021. Impact of the Southern Ecuadorian Andes on Oxygen and Hydrogen Isotopes in Precipitation. Frontiers in Earth Science 9, 664590.

Goldsmith, Y., Polissar, P.J., deMenocal, P.B., Broecker, W.S., 2019. Leaf Wax δD and δ13C in Soils Record Hydrological and Environmental Information Across a Climatic Gradient in Israel. Journal of Geophysical Research: Biogeosciences 124, 2898–2916.

González-Pérez, J.A., González-Vila, F.J., Almendros, G., Knicker, H., 2004. The effect of fire on soil organic matter—a review. Environment International 30, 855–870.

Harrington, C.A., Ford, K.R., Clair, J.B.S., 2016. Phenology of Pacific Northwest Tree Species. Tree Planters' Notes 59, 76–85.

Howard, S., 2014. Variation in chain-length of leaf wax *n*-alkanes in plants and soils across Australia (Honours). University of Adelaide.

Hren, M.T., Pagani, M., Erwin, D.M., Brandon, M., 2010. Biomarker reconstruction of the early Eocene paleotopography and paleoclimate of the northern Sierra Nevada. Geology 38, 7–10.

Huang, Y., Eglinton, G., Ineson, P., Latter, P.M., Bol, R., Harkness, D.D., 1997. Absence of carbon isotope fractionation of individual *n*-alkanes in a 23-year field decomposition experiment with Calluna vulgaris. Organic Geochemistry 26, 497–501.

IAEA/WMO Global Network of Isotopes in Precipitation, 2017, The GNIP Database, http://www.iaea.org/water.

Jarrett, A.J.M., Cox, G.M., Brocks, J.J., Grosjean, E., Boreham, C.J., Edwards, D.S., 2019. Microbial assemblage and palaeoenvironmental reconstruction of the 1.38 Ga Velkerri Formation, McArthur Basin, northern Australia. Geobiology 17, 360–380.

Jia, G., Bai, Y., Ma, Y., Sun, J., Peng, P., 2015. Paleoelevation of Tibetan Lunpola basin in the Oligocene–Miocene transition estimated from leaf wax lipid dual isotopes. Global and Planetary Change 126, 14–22.

Jia, G., Wei, K., Chen, F., Peng, P., 2008. Soil *n*-alkane δD vs. altitude gradients along Mount Gongga, China. Geochimica et Cosmochimica Acta 72, 5165–5174.

Kahmen, A., Dawson, T.E., Vieth, A., Sachse, D., 2011. Leaf wax *n*-alkane δD values are determined early in the ontogeny of Populus trichocarpa leaves when grown under controlled environmental conditions: Early determination of leaf wax *n*-alkane δD values. Plant, Cell & Environment 34, 1639–1651.

Kikuchi, T., Suzuki, N., Saito, H., 2010. Change in hydrogen isotope composition of *n*-alkanes, pristane, phytane, and aromatic hydrocarbons in Miocene siliceous mudstones with increasing maturity. Organic Geochemistry 41, 940–946.

Kim, K., Lee, X., 2011. Isotopic enrichment of liquid water during evaporation from water surfaces. Journal of Hydrology 399, 364–375.

Kowalewski, M., Bambach, R.K., 2008. The Limits of Paleontological Resolution, in: High-Resolution Approaches in Stratigraphic Paleontology, Topics in Geobiology. Springer, Dordrecht, pp. 1–48.

Kumar, U.S., Kumar, B., Rai, S.P., Sharma, S., 2010. Stable isotope ratios in precipitation and their relationship with meteorological conditions in the Kumaon Himalayas, India. Journal of Hydrology 391, 1–8.

Ladd, S.N., Maloney, A.E., Nelson, D.B., Prebble, M., Camperio, G., Sear, D.A., Hassall, D., Langdon, P.G., Sachs, J.P., Dubois, N., 2021. Leaf Wax Hydrogen Isotopes as a Hydroclimate Proxy in the Tropical Pacific. JGR Biogeosciences 126, e2020JG005891.

Lane, C.S., 2017. Modern *n*-alkane abundances and isotopic composition of vegetation in a gymnosperm-dominated ecosystem of the southeastern U.S. coastal plain. Organic Geochemistry 105, 33–36.

Lin, J., Dai, J., Zhuang, G., Jia, G., Zhang, L., Ning, Z., Li, Y., Wang, C., 2020. Late Eocene–Oligocene High Relief Paleotopography in the North Central Tibetan Plateau: Insights From Detrital Zircon U–Pb Geochronology and Leaf Wax Hydrogen Isotope Studies. Tectonics 39.

Liu, J., An, Z., 2019. Variations in hydrogen isotopic fractionation in higher plants and sediments across different latitudes: Implications for paleohydrological reconstruction. Science of the Total Environment 650, 470–478.

Lyons, C.P., 1999. Trees and Shrubs of Washington, 1st ed, Lone Pine Field Guide. Lone Pine Publishing, Canada.

Lyons, C.P., Merilees, B., 1995. Trees, Shrubs, and Flowers to Know in Washington and British Columbia, 6th ed. Lone Pine Publishing, Canada.

Marshall, C.P., Love, G.D., Snape, C.E., Hill, A.C., Allwood, A.C., Walter, M.R., Van Kranendonk, M.J., Bowden, S.A., Sylva, S.P., Summons, R.E., 2007. Structural characterization of kerogen in 3.4Ga Archaean cherts from the Pilbara Craton, Western Australia. Precambrian Research 155, 1–23.

Martínez-Vilalta, J., Poyatos, R., Aguadé, D., Retana, J., Mencuccini, M., 2014. A new look at water transport regulation in plants. New Phytologist 204, 105–115.

Massa, C., Beilman, D.W., Nichols, J.E., Timm, O.E., 2021. Central Pacific hydroclimate over the last 45,000 years: Molecular-isotopic evidence from leaf wax in a Hawai‘i peatland. Quaternary Science Reviews 253, 106744.

Mayr, S., Hacke, U., Schmid, P., Schwienbacher, F., Gruber, A., 2006. Frost Drought in Conifers at the Alpine Timberline: Xylem Dysfunction and Adaptations. Ecology 87, 3175–3185.

McFarlin, J.M., Axford, Y., Masterson, A.L., Osburn, M.R., 2019. Calibration of modern sedimentary δ2H plant wax-water relationships in Greenland lakes. Quaternary Science Reviews 225, 105978.

McInerney, F.A., Helliker, B.R., Freeman, K.H., 2011. Hydrogen isotope ratios of leaf wax *n*-alkanes in grasses are insensitive to transpiration. Geochimica et Cosmochimica Acta 75, 541–554.

Meinzer, F.C., Woodruff, D.R., Marias, D.E., Mcculloh, K.A., Sevanto, S., 2014. Dynamics of leaf water relations components in co-occurring iso- and anisohydric conifer species: Dynamics of leaf water relations components. Plant, Cell & Environment 37, 2577–2586.

Meyers, P.A., Leenheer, M.J., Bourbonniere, R.A., 1995. Diagenesis of vascular plant organic matter components during burial in lake sediments. Aquatic Geochemistry 1, 35–52.

Minder, J., Mote, Philip W., Lundquist, Jessica D., 2010. Surface temperature lapse rates over complex terrain: Lessons from the Cascade Mountains. JGR Atmospheres 115, 1–13.

Mook, W.G., 2001. Environmental Isotopes in the Hydrological Cycle: Principles and Applications, IHP-V Technical Documents in Hydrology. UNESCO-IAEA.

Mook, W.G., Groeneveld, D.J., Brouwn, A.E., Van Ganswijk, A.J., 1974. Analysis of a run-off hydrograph by means of natural 18O, in: Proc. Conf. Isotope Techniques in Groundwater Hydrology. IAEA, Vienna.

Mulch, A., Graham, S.A., Chamberlain, C.P., 2006. Hydrogen Isotopes in Eocene River Gravels and Paleoelevation of the Sierra Nevada. Science 313, 87–89.

Nelson, D.B., Knohl, A., Sachse, D., Schefuß, E., Kahmen, A., 2017. Sources and abundances of leaf waxes in aerosols in central Europe. Geochimica et Cosmochimica Acta 198, 299–314.

Nelson, D.B., Ladd, S.N., Schubert, C.J., Kahmen, A., 2018. Rapid atmospheric transport and large-scale deposition of recently synthesized plant waxes. Geochimica et Cosmochimica Acta 222, 599–617.

Nelson, D.B., Sachs, J.P., 2013. Concurrent purification of sterols, triterpenols and alkenones from sediments for hydrogen isotope analysis using high performance liquid chromatography. Organic Geochemistry 64, 19–28.

Newberry, S.L., Kahmen, A., Dennis, P., Grant, A., 2015. *n*-Alkane biosynthetic hydrogen isotope fractionation is not constant throughout the growing season in the riparian tree Salix viminalis. Geochimica et Cosmochimica Acta 165, 75–85.

Nguyen Tu, T.T., Egasse, C., Anquetil, C., Zanetti, F., Zeller, B., Huon, S., Derenne, S., 2017. Leaf lipid degradation in soils and surface sediments: A litterbag experiment. Organic Geochemistry 104, 35–41.

Niedermeyer, E.M., Forrest, M., Beckmann, B., Sessions, A.L., Mulch, A., Schefuß, E., 2016. The stable hydrogen isotopic composition of sedimentary plant waxes as quantitative proxy for rainfall in the West African Sahel. Geochimica et Cosmochimica Acta 184, 55–70.

Nieto-Moreno, V., Rohrmann, A., van der Meer, M.T.J., Sinninghe Damsté, J.S., Sachse, D., Tofelde, S., Niedermeyer, E.M., Strecker, M.R., Mulch, A., 2016. Elevation-dependent changes in *n*-alkane δD and soil GDGTs across the South Central Andes. Earth and Planetary Science Letters 453, 234–242.

Pedentchouk, N., Sumner, W., Tipple, B., Pagani, M., 2008. δ13C and δD compositions of *n*-alkanes from modern angiosperms and conifers: An experimental set up in central Washington State, USA. Organic Geochemistry 39, 1066–1071.

Poage, M.A., Chamberlain, C.P., 2001. Empirical relationships between elevation and the stable isotope composition of precipitation and surface waters: Considerations for studies of paleoelevation change. American Journal of Science 301, 1–15.

Pojar, J., MacKinnon, A., 2014. Plants of the Pacific Northwest Coast: Washington, Oregon, British Columbia, and Alaska, Revised. ed. Lone Pine Publishing, Canada.

Polissar, P.J., Freeman, K.H., Rowley, D.B., McInerney, F.A., Currie, B.S., 2009. Paleoaltimetry of the Tibetan Plateau from D/H ratios of lipid biomarkers. Earth and Planetary Science Letters 287, 64–76.

Poulos, H.M., Berlyn, G.P., Mills, S.A., 2012. Differential stress tolerance of four pines (Pinaceae) across the elevation gradient of the San Bernardino Mountains, Southern California, USA. The Journal of the Torrey Botanical Society 139, 96–108.

Reich, P.B., Rich, R.L., Lu, X., Wang, Y.-P., Oleksyn, J., 2014. Biogeographic variation in evergreen conifer needle longevity and impacts on boreal forest carbon cycle projections. Proceedings of the National Academy of Sciences 111, 13703–13708.

Roe, G.H., 2005. Orographic Precipitation. Annual Review of Earth and Planetary Sciences 33, 645–671.

Roe, G.H., Baker, M.B., 2006. Microphysical and Geometrical Controls on the Pattern of Orographic Precipitation. Journal of the Atmospheric Sciences 63, 861–880.

Sachse, D., Billault, I., Bowen, G.J., Chikaraishi, Y., Dawson, T.E., Feakins, S.J., Freeman, K.H., Magill, C.R., McInerney, F.A., van der Meer, M.T.J., Polissar, P., Robins, R.J., Sachs, J.P., Schmidt, H.-L., Sessions, A.L., White, J.W.C., West, J.B., Kahmen, A., 2012. Molecular Paleohydrology: Interpreting the Hydrogen-Isotopic Composition of Lipid Biomarkers from Photosynthesizing Organisms. Annual Review of Earth and Planetary Sciences 40, 221–249.

Sachse, D., Dawson, T.E., Kahmen, A., 2015. Seasonal variation of leaf wax *n*-alkane production and δ2H values from the evergreen oak tree, Quercus agrifolia. Isotopes in Environmental and Health Studies 51, 124–142.

Schemmel, F., Mikes, T., Mulch, A., 2013. The impact of topography on isotopes in precipitation across the Central Anatolian Plateau (Turkey). American Journal of Science 313, 61–80.

Schwab, V.F., Garcin, Y., Sachse, D., Todou, G., Séné, O., Onana, J.-M., Achoundong, G., Gleixner, G., 2015. Effect of aridity on δ13C and δD values of C3 plant- and C4 graminoid-

derived leaf wax lipids from soils along an environmental gradient in Cameroon (Western Central Africa). Organic Geochemistry 78, 99–109.

Schlanser, K.F., Diefendorf, A.F., West, C.K., Greenwood, D.R., Basinger, J.F., Meyer, H.W., Lowe, A.J., and Naake, H.H., 2020. Conifers are a major source of sedimentary leaf wax *n*-alkanes when dominant in the landscape: Case studies from the Paleogene. Organic Geochemistry 147, 1-17.

Shepherd, T., Wynne Griffiths, D., 2006. The effects of stress on plant cuticular waxes: Tansley review. New Phytologist 171, 469–499.

Shi, Z., Allison, S.D., He, Y., Levine, P.A., Hoyt, A.M., Beem-Miller, J., Zhu, Q., Wieder, W.R., Trumbore, S., Randerson, J.T., 2020. The age distribution of global soil carbon inferred from radiocarbon measurements. Nature Geoscience 13, 555–559.

Smith, F.A., Freeman, K.H., 2006. Influence of physiology and climate on δD of leaf wax *n*-alkanes from C3 and C4 grasses. Geochimica et Cosmochimica Acta 70, 1172–1187.

Tardieu, F., Simmoneau, T., 1998. Variability among species of stomatal control under fluctuating soil water status and evaporative demand: modelling isohydric and anisohydric behaviours. Journal of Experimental Botany 49, 419–432.

Taylor, A.B., 1972. The vertical variations of the isotopic concentrations of tropospheric water vapour over continental Europe and their relationship to tropospheric structure (No. INS-R-107). New Zealand Institute of Nuclear Science.

Tipple, B.J., Berke, M.A., Doman, C.E., Khachaturyan, S., Ehleringer, J.R., 2013. Leaf-wax *n*-alkanes record the plant-water environment at leaf flush. Proceedings of the National Academy of Sciences 110, 2659–2664.

Tipple, B.J., Pagani, M., 2013. Environmental control on eastern broadleaf forest species' leaf wax distributions and D/H ratios. Geochimica et Cosmochimica Acta 111, 64–77.

Trumbore, S., 2000. Age of Soil Organic Matter and Soil Respiration: Radiocarbon Constraints on Belowground C Dynamics. Ecological Applications 10, 399–411.

Voelker, S.L., DeRose, R.J., Bekker, M.F., Sriladda, C., Leksungnoen, N., Kjelgren, R.K., 2018. Anisohydric water use behavior links growing season evaporative demand to ring-width increment in conifers from summer-dry environments. Trees 32, 735–749.

Vogel, J.C., Lerman, J.C., Mook, W.G., 1975. Natural isotopes in surface and groundwater from Argentina. Hydrological Sciences Bulletin XX, 203–221.

Volk, H., George, S.C., Dutkiewicz, A., Ridley, J., 2005. Characterisation of fluid inclusion oil in a Mid-Proterozoic sandstone and dolerite (Roper Superbasin, Australia). Chemical Geology 223, 109–135.

Warren, C.R., Livingston, N.J., Turpin, D.H., 2003. Responses of gas exchange to reversible changes in whole-plant transpiration rate in two conifer species. Tree Physiology 23, 793–803.

West, A.G., Hultine, K.R., Jackson, T.L., Ehleringer, J.R., 2007. Differential summer water use by Pinus edulis and Juniperus osteosperma reflects contrasting hydraulic characteristics. Tree Physiology 27, 1711–1720.

Yang, H., Liu, W., Leng, Q., Hren, M.T., Pagani, M., 2011. Variation in *n*-alkane δD values from terrestrial plants at high latitude: Implications for paleoclimate reconstruction. Organic Geochemistry 42, 283–288.

Yanuskiewicz, E.A., Lane, C.S., Horn, S.P., Johanson, E.N., Gamble, D.W., 2022. Compound-specific stable carbon and hydrogen isotope analyses of late-Holocene vegetation and precipitation change at Laguna Los Mangos, Costa Rica. Quaternary International 607, 22–34.

Yurtsever, Y., 1975. Worldwide survey of isotopes in precipitation. International Atomic Energy Agency (IAEA), Vienna.

Zech, M., Pedentchouk, N., Buggle, B., Leiber, K., Kalbitz, K., Marković, S.B., Glaser, B., 2011. Effect of leaf litter degradation and seasonality on D/H isotope ratios of *n*-alkane biomarkers. Geochimica et Cosmochimica Acta 75, 4917–4928.

Zhang, P., Liu, W., 2011. Effect of plant life form on relationship between δD values of leaf wax *n*-alkanes and altitude along Mount Taibai, China. Organic Geochemistry 42, 100–107.

Zhang, X., Xu, B., Günther, F., Mügler, I., Lange, M., Zhao, H., Li, J., Gleixner, G., 2017. Hydrogen isotope ratios of terrestrial leaf wax *n*-alkanes from the Tibetan Plateau: Controls on apparent enrichment factors, effect of vapor sources and implication for altimetry. Geochimica et Cosmochimica Acta 211, 10–27.

Zhuang, G., Brandon, M.T., Pagani, M., Krishnan, S., 2014. Leaf wax stable isotopes from Northern Tibetan Plateau: Implications for uplift and climate since 15 Ma. Earth and Planetary Science Letters 390, 186–198.

Zhuang, G., Pagani, M., Chamberlin, C., Strong, D., Vandergoes, M., 2015. Altitudinal shift in stable hydrogen isotopes and microbial tetraether distribution in soils from the Southern Alps, NZ: Implications for paleoclimatology and paleoaltimetry. Organic Geochemistry 79, 56–64.